

Permafrost saline water and Early to Mid-Holocene permafrost aggradation in Svalbard

Dotan Rotem^{1,2}, Vladimir Lyakhovsky³, Hanne Hvidtfeldt Christiansen², Yehudit Harlavan³, Yishai Weinstein¹

¹Department of Geography and Environment, Bar-Ilan University, Ramat-Gan, 52900, Israel.

²Arctic geophysics Department, the University Centre in Svalbard, UNIS, Longyearbyen 9170, Norway.

³Geological Survey of Israel, 32 Yesha'yahu Leibowitz, Jerusalem 9692100, Israel.

Correspondence to: dotanrotem1969@gmail.com

Abstract. Deglaciation in Svalbard was followed by seawater ingress and deposition of marine (deltaic) sediments in fjord valleys, while elastic rebound resulted in fast land uplift and the exposure of these sediments to the atmosphere, in which the formation of epigenetic permafrost formed. This was then followed by the accumulation of aeolian sediments, with syngenetic permafrost formation. ~~The permafrost~~ Permafrost was drilled and studied in the eastern Adventdalen valley, Svalbard, 3-4 km from the maximum up-valley reach of post-deglaciation seawater ingress, and its ground ice was analyzed geochemically for its chemistry. While ground ice in the syngenetic part is basically fresh, the epigenetic part has a frozen fresh-saline water interface (FSI), with chloride concentrations increasing from the top of the epigenetic part (at depth of 5.5 m depth) to about 15% that of seawater at 11 m depth. We applied a one-dimensional freezing model to examine the rate of top-down permafrost formation, which could accommodate with the observed frozen FSI. The model examined permafrost development under different scenarios of mean average air temperature, water-freezing temperature and the degree of pore-water freezing. We found that even at the relatively high air temperatures of the Early to mid-Holocene, permafrost could aggrade quite fast down to 15 to 33 m (the whole sediment fill of 20 m at this location) within 200 years, therefore, this, in turn, allowed freezing and preservation and freezing of the fresh-saline water interface despite of the relatively fast rebound rate, which apparently resulted in an and the resultant resulting increase in topographic gradients toward the sea. This permafrost aggradation rate could also be enhanced was possible due to non-complete pore water freezing, which possibly lead to slightly faster aggradation, resulting in the freezing of the entire marine section at that location (23 m) within less than 200 years. We conclude that freezing must have started immediately after the exposure of the marine sediment to atmospheric conditions.

1. Introduction

30 Cycles of global warming and cooling are well documented in the geological history (e.g., Imbrie et al., 1993; Benn & Evans, 2014; Arnscheidt & Rothman, 2020). During the Pleistocene, these cycles followed Northern Hemisphere glaciation and deglaciation, which influenced both marine and land temperatures (Park et al., 2019). This also affected the extent of cryotic conditions in the periglacial environment (e.g. Murton, 2021), i.e., the distribution of permafrost, which currently covers 22% of the ~~northern-Northern~~
35 ~~hemisphere-Hemisphere~~ land areas (Obu et al., 2019). While temperatures during the Holocene were significantly higher than during the Last Glacial period, the retreat of glaciers and the follow-up elastic rebound and exposure of new land in the Arctic and the sub-Arctic environment allowed freezing and the aggradation of permafrost (e.g. Landvik et al., 1988). Nevertheless, the relatively high temperatures during the Early and the mid-Holocene warm period raise questions about the timing of initiation and the
40 extent of this process (e.g. Landvik et al., 1988; Humlum, 2005).

In Svalbard (Fig. 1), the fast retreat of glaciers during the end of Late-Pleistocene into the beginning of the Holocene resulted in the ingression of seawater in fjord valleys, which was followed by gradual uplifting and exposure due to elastic rebound. This resulted in epigenetic permafrost aggradation followed by the deposition of ~~fluvatile-fluvial~~ and aeolian sediments, and the formation of syngenetic
45 permafrost during the last ca. 4 ka (Gilbert et al., 2018). In the present study, we use the presence of saline water in the epigenetic permafrost to constrain the timing of freezing.

Permafrost is a soil or rock, which has been below ~~zero temperature~~ 0°C for at least two consecutive years (French, 2017). While winter freezing of the ground is common in a large extent of land areas, the existence of permafrost and its aggradation depends on the annual energy balance between atmosphere and the land (Black, 1954). Accordingly, permafrost develops when the land heat loss during winter
50 exceeds the gain during the summer for long enough time. This is controlled by both seasonal solar radiation and the soil/rock thermal properties. Heat exchange between soil and the atmosphere is also strongly affected by land cover, whereby permafrost is usually ~~is~~ not developed neither under the sea nor beneath warm-based ~~d~~ glaciers (Waller et al., 2012). Nevertheless, permafrost can be present
55 associated with ~~fern in taliks beneath lagoons as well as beneath bottom-fast ice conditions in shallow~~ water (Solomon et al., 2008). The extent and depth of permafrost can be significantly reduced by thick vegetation or snow cover (e.g. Grünberg et al., 2020).

60 During the ~~Last-last Glacial-glacial Maximum cycle(LGM)~~, the Barents Sea and the Svalbard area (Fig. 1) were covered by one to three ice caps (Mangerud et al., 2002; Patton et al., 2017). Glacier retreat ~~was-has been~~ followed since by elastic rebound, which is well documented in Svalbard (Bondevik et al., 1995; Lønne & Nemeč, 2004; Sessford et al., 2015), with a land rise of up to 130 m in eastern Svalbard and 65 m in the western part of the archipelago (Forman, 2004). In western Svalbard, the ~~locus-focus~~ of this study, research indicates a fast land rise of 19-15 mm y⁻¹ during Early to the mid-Holocene (11.7 – 8.2 ka BP), which decreased to 5 - 4 mm y⁻¹ toward the end of mid-Holocene (Salvigsen, 1984; Sessford et al., 2015) and ca. 1 mm y⁻¹ during the late Holocene (last 4 ka, e.g. Forman et al., 2004).

Land uplift and exposure is accompanied by the establishment of a surficial drainage system, as well as the development of a groundwater flow network, which strongly depends on the rate of permafrost deepening (Edmunds et al., 2001). The permeability of frozen soils is greatly reduced (Burt and Williams, 1976; Cochand et al., 2019), such that extensive permafrost prevents penetrating of surface water and recharging of groundwater (McEwen & de Marsily, 1991). While in sporadic and discontinuous permafrost, groundwater flow is possible through non-frozen sections or taliks, flow is practically impossible through continuous permafrost land areas (Lemieux et al., 2008; Walvoord and Kurylyk, 2016), while it may be active in sub-permafrost zones. Flow may also be enhancing cryopegs which holds overcooled liquid brines (Ahonen 2001), or move among existing cryopegs (Iwahana et al., 2021). 75 Although Cryopegs was describeidentified in Adventdalen (Tavacoli et al., 2021), water paths were not yet described. Water flow along faults in continuous permafrost ~~was~~has been described in Adventdalen Svalbard in relation to pingos (Hornum et al., 2021).

According to the Ghyben-Hertzberg approximation (Bear & Dagan 1964; Verruijt 1968), depth from seawater level to the fresh-saline water interface should be about 1:40 of the groundwater head above sea level. This ratio increases with decreasing salinity of saline water. With typical Early to mid-Holocene rebound rates of 15 to 4.5 mm y⁻¹ (Sessford et al., 2015), and assuming that the groundwater table (saturated conditions) followed the topography, the fresh-saline interface is expected to be pushed downwards to as deep as 120 to 36 m respectively, within 200 years after exposure. A Ggroundwater table of 1 m below the surface would result in a delay of 100 to 200 years, but also in this case a sediment section of tens of meters will be completely flushed within several hundred years. This ~~occure-is~~ unless 85 sediment freezing practically halts flow in the subsurface.

~~In-The objective of~~ this paper is to ~~we~~ test theis presented hypothesis by studying the ground ice geochemistry of a permafrost core from Adventdalen, Svalbard, and by using a 1-D numerical heat

transfer model to simulate permafrost aggradation under various surface temperature conditions and degrees of freezing.

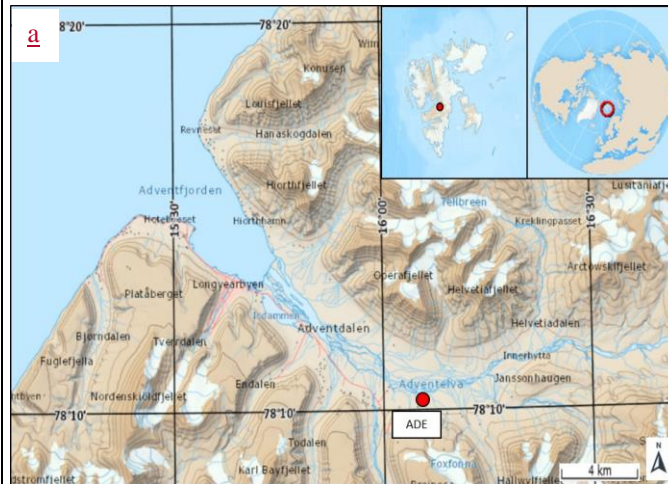
2. Study site

Adventdalen is a U-shaped glacially eroded valley located in western Spitsbergen, Svalbard, centred on 78.110N, 16.180E (Fig. 1a). During the last glacial cycle, the valley was eroded to the basement, which was then covered by glacial deposits (Elverhøi et al., 1995; Gilbert et al., 2018). This was followed by deglaciation, which was completed ca. 10.5 ka BP (Mangerud et al., 1992; Svendsen & Mangerud, 1997; Lønne & Lyså, 2005; Farnsworth et al., 2020). Deglaciation was followed by up-valley seawater ingression, up to 13.5 km from the current end of the fjord (Cable et al., 2018; Lønne & Nemec, 2004) and subsequent valley infilling with sediment and a delta front prograding downvalley. ~~the deposition of foredelta and deltaic deposits.~~ Elastic rebound resulted in the exposure of the eastern part of the valley before 9.5 ka BP, which progressed down-valley, arriving at the current coastline location at about 4 ka (Gilbert et al., 2018). ~~The Ex~~posed surface was first covered by fluvial sediments, followed by aeolian deposits during 4-2 ka (Gilbert et al., 2018). Permafrost in Svalbard, both epigenetic and syngenetic, is continuous and is estimated to be >100 m thick in the valleys (Humlum, 2005). ~~The A~~active-layer thickness is commonly 60–100 cm in the valley bottom sediments (Christiansen and Humlum, 2003; Gilbert et al., 2018; Weinstein et al., 2019; Strand et al., 2020).

Meteorological data is measured continuously for more than 100 years at the Svalbard Airport (e.g. Nordli et al., 2020), located on the Adventfjorden coast, ca. 12 km northwest of our study site. Mean annual air temperature (hereafter MAAT) was -5.9 °C from 1971 to 2000, although in 2018 it was merely -1.8 °C. Mean annual precipitation during 1971-2000 was 196 mm, while in 2018 it was 177 mm (Strand et al., 2021). MAAT and sea surface temperature during Early to the mid-Holocene were/was 2-4 °C higher than today, as suggested by marine molluscs/mollusc's shells (Mangerud & Svendsen, 2018), lacustrine alkenons (van der Bilt et al., 2018), flora DNA (Alsos et al., 2016) and models incorporating physical and biological considerations (e.g. Park et al., 2019). Since the mid-Holocene, a continuous decline in mean annual air temperature (hereafter MAAT) is recorded, changing-which changed into a fast temperature rise during the last several decades (e.g. Christiansen et al., 2013).

The study site, Adventdalen East (ADE), is located on a river terrace (78.1722° N 16.0613° E), 9.8 km km upvalley from the Adventfjorden at 23 m a.s.l (Fig. 1a and b). ~~We drilled inat the exactsame S1~~

120 location of [Gilbert et al., \(2018\)](#). The Pp permafrost section (valley-fill sediments) at the ADE site (ca.
 20+ m) consists of a syngenetic part from 1.0 ~~to~~ 5.5 m depth, which includes a shallow 1.5 m of
 125 syngenetic fine-grained aeolian deposits and thick ice bodies of segregation ice intruded above fluvial
gravel channel fill ([Gilbert et al., 2018](#)). Below 5.5 m the epigenetic permafrost consists of, underlain by 3-
4-m of fluvial ~~the~~ sediments (mud and pebbles, ice-rich). This is underlain by back-delta, deltaic and fore-
 delta sediments (5.5-17.5 m), which cover glacial sand deposits (17.5-20 m); ([Gilbert et al., 2018](#)), -all of
 130 which are part of the epigenetic permafrost. The study site was deglaciated by 11.3 ka and emerged
 above seawater at 9.2 ka ([Gilbert et al., 2018](#)), exposing it to atmospheric conditions then, which allowed
 the development of a groundwater system on one hand and possibly the aggradation of permafrost on
 the other hand.



130



Figure 1. (a) Study site ADE is located at the Adventdalen, Svalbard, on a river terrace. Map provided with courtesy of Norwegian Polar Institute. (b) Drilling at ADE, spring 2017 top. Cores samples before processing at UNIS cold room lab, bottom.

135

3. Methods

Two cores, placed 0.5 m apart, one 13 m and the other 9 m long, were retrieved at ADE in March 2017, using the UNIS permafrost drill-rig (Gilbert et al., 2015), which has core barrels of 43 mm diameter (ID). Core length, borehole depth, core condition, and gravel content were recorded in the field. Retrieved

140

core sections were placed in plastic bags and marked with a serial number and an arrow pointing towards the core top. Cores were stored at -18°C in a freezer at UNIS until processing. Cores were sectioned in a cold room (-5°C) to 0.5 m depth intervals (Fig 1b). Intervals of the same depth in the two cores were combined ~~in order~~ to gain enough ground-ice per section for Ra isotope measurements. Samples were first scraped and then crashed to small chips, which were placed in 250 ml centrifuge tubes. Ra-free water (up to 40 ml) was added to some of the tubes, ~~in order~~ to facilitate the extraction of pore fluid. Samples were then thawed in a microwave set to 600 W for 2 min, followed by centrifuging for 8 min (11,000 RPM, high G) to separate thawed water from the soil. Extracted water was run through 3 µm, followed by 0.45 µm filters. Most of the water was used for Ra isotopes analysis (see Weinstein et al., 2019), while 30-60 ml was used for chemistry analyses. Water of the added Ra-free water was analysed to correct for element concentrations. Major elements were analysed in the Geological Survey of Israel (GSI) by ICP-AES (Optima 3000), where Sc was added as an internal standard, whereas Cl⁻ and SO₄²⁻ was determined by potentiometer titration, using Metrohm 702 SM Titrino Titrator connected to a chlorine electrode. The error for all majors is considered less than 5%.

4. Ground ice Chemistry

Major elements of thawed ground ice are presented in Table 1 and concentration profiles of Cl⁻, Na²⁺ and SO₄²⁻ are shown in Fig. 2 a-c. While the salinity of ground ice in the syngenetic permafrost is that of fresh water (e.g. Cl⁻: 10-74 mg/L, Na²⁺: 10-33 mg/L and SO₄²⁻: 9-31 mg/L), epigenetic permafrost ground ice demonstrates a trend of increasing concentrations down to 9-12 m depth: 440-3600, 80-2700 and 150-740 mg/L of Cl⁻, Na²⁺ and SO₄²⁻, respectively. Between 9-12 m, concentrations are quite scattered, and the increasing pattern is less clear. While the Cl⁻ content (Fig. 2a) of the ground ice is no more than 15% seawater salinity, and the salinity of a deeper-seated saline water end member could be significantly higher ~~than seawater~~, the observed increased salinity clearly ~~points to the location of~~ presents a fresh-saline water interface.

The ionic ratio of Na²⁺ to Cl⁻ in both epigenetic and the syngenetic permafrost mostly exceeds 1 (Fig. 2d), significantly higher than in seawater (0.86), which is probably the result of sediment dissolution (e.g. of micas), since ion exchange should result in either a conservative behaviour (during freshening, as is the case in the ADE marine section) or in Na⁺ depletion (in the case of salinization, e.g. Russak and Sivan, 2010). On the other hand, SO₄/Cl⁻ in the epigenetic permafrost is close to that of seawater (Fig.

170 2f), implying a relative conservative behaviour. Nevertheless, SO_4/Cl^- in the syngenetic part is very variable (Fig. 2f), reaching ratios as high as 2, which could be due to shale dissolution (Hindshaw et al., 2016; Cabel et al., 2018). ~~Higher than seawater ratios of what were also recorded in the upper 2 m of the epigenetic permafrost.~~ High concentration of SO_4 was also recorded in sub-permafrost (Pingo) water, which was attributed to gypsum dissolution (Hodson et al., 2020). $-\text{Ca}/\text{Cl}$ decreases with depth in the syngenetic permafrost and is very low (<0.01) in the epigenetic permafrost (Fig. 2e), which is in agreement with freshening experiments [in fresh-saline water zones](#) (Russak and Sivan 2010). The high ratio of Ca/Cl and SO_4/Cl at -5.45-m depth is enigmatic and ~~may present paleo active layer - permafrost table zone were major and minor elements concentrate (e.g. Cary and Mayland, 1972; Kokelj et al., 2002) but it should be further studied.~~

180

Table 1. Major elements (mg/L) of grownd-ice samples of the ADE core.

| Sample name | Depth (m) | Permafrost Type ₁ | Cl^- | Br | SO_4^{2-} | SiO_2 | Na^+ | K^+ | Sr | Ca^{2+} | Mg^{2+} | Freezing state of sample ₂ |
|--|-----------|------------------------------|---------------|------|--------------------|----------------|---------------|--------------|-----|------------------|------------------|---------------------------------------|
| Sea water conc.₂ | | | 19.354 | 67.3 | 2.712 | | 10.760 | 399 | 7.9 | 412 | 1.290 | |
| DR-AD-55 | -1.3 | Syngenetic | 27.1 | 0.5 | 19.0 | 13.0 | 10.7 | 17.0 | 0.2 | 5.4 | 15.1 | Frozen |
| DR-AD-58 | -2.1 | Syngenetic | 12.8 | 0.6 | 30.7 | 14.0 | 19.8 | 4.1 | 0.4 | 8.8 | 27.8 | Frozen |
| DR-AD-52 | -2.9 | Syngenetic | 74.1 | 0.7 | 8.9 | 9.0 | 13.6 | 44.7 | 0.6 | 12.7 | 35.2 | Frozen-icy |
| DR-AD-57 | -3.3 | Syngenetic | 13.9 | 0.5 | 27.9 | 5.9 | 32.6 | 4.4 | 0.1 | 3.6 | 7.6 | Frozen-icy |
| DR-AD-56 | -3.5 | Syngenetic | 10.0 | 0.3 | 12.3 | 5.3 | 13.3 | 4.5 | 0.1 | 1.5 | 2.6 | Frozen-icy |
| DR-AD-61 | -4.0 | Syngenetic | 14.5 | 0.7 | 13.0 | 11.6 | 9.5 | 5.2 | 0.2 | 3.6 | 8.8 | Frozen |
| DR-AD-63 | -4.7 | Syngenetic | 26.8 | | 11.6 | 30.0 | 12.8 | 13.6 | 0.1 | 1.7 | 2.6 | Frozen |
| DR-AD-59 | -5.5 | Epigenetic | 67.4 | 0.6 | 146.6 | 20.9 | 83.3 | 16.0 | 0.5 | 13.6 | 27.0 | Partly frozen |
| DR-AD-53 | -6.3 | Epigenetic | 438.1 | 1.9 | 116.1 | 19.4 | 422.0 | 6.7 | 0.5 | 14.2 | 6.1 | Frozen |
| DR-AD-64 | -7.1 | Epigenetic | 847.0 | | 369.5 | 38.1 | 828.7 | 22.7 | 0.1 | 11.6 | | Frozen |
| DR-AD-65 | -8.3 | Epigenetic | 1678.4 | | 465.1 | 21.2 | 1296.3 | 29.1 | 0.1 | 0.5 | | Frozen |
| DR-AD-67 | -8.8 | Epigenetic | 3677.6 | | 570.4 | 25.0 | 1680.1 | 55.6 | 0.1 | 2.2 | | Partly frozen |
| DR-AD-54 | -9.4 | Epigenetic | 2145.1 | 7.9 | 508.2 | 9.1 | 2497.5 | 194.6 | 0.3 | 17.0 | | Partly frozen |

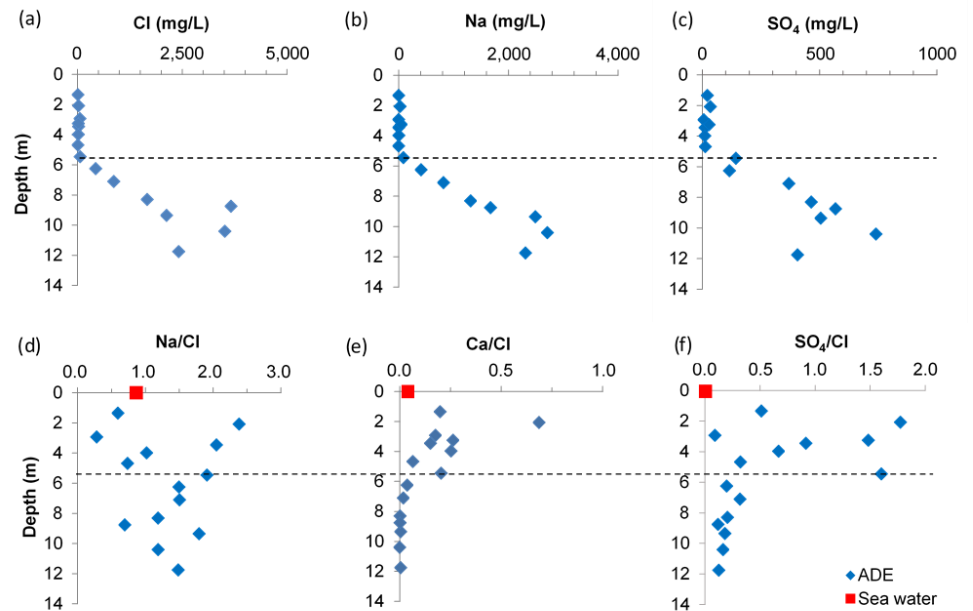
| | | | | | | | | | | | |
|----------|-------|------------|--------|-----|-------|------|--------|------|-----|------|---------------|
| DR-AD-66 | -10.4 | Epigenetic | 3500.4 | | 738.9 | 24.8 | 2705.8 | 42.4 | 0.4 | 9.5 | Partly frozen |
| DR-AD-60 | -11.8 | Epigenetic | 2412.6 | 7.0 | 408.1 | 20.5 | 2319.8 | 98.0 | 0.6 | 18.3 | Partly frozen |

¹ after Gilbert et al., 2018

² after de Baar et al., 2017, Salinity of 35%

³ Freezing state as recorded in the field

185



190

Figure 2. Major element concentrations in ground ice from Adventdalen-East (ADE) deep drillhole: (a) Cl⁻, (b) Na⁺ & (c) SO₄²⁻ in mg/L. Figures (d) - (f) present selected equivalent ratios along the profile. Dashed line separates the syngenetic and the epigenetic permafrost (Gilbert et al., 2018).

195 5. Model of permafrost formation

5.1 Conceptual model

To study the ~~potential~~ rate of ~~the~~ permafrost formation, we developed a numerical model that solves the temperature distribution in space and time and freezing front progression, ~~i.e.~~ Stefan solution (e.g., Šarler, 1995). Considering low horizontal temperature variations, the problem ~~is-was~~ reduced to one dimensional depth-dependent heat transfer with moving internal phase transition boundary. Various analytical and numerical methods have been developed to obtain stable solution of the Stefan problem (e.g., Crank, 1984). However, unlike the simple and clean single component systems, many natural systems, including water saturated porous rocks, change their phases under a specified temperature range rather than isothermally (Lunardini, 1987; Růhaak et al., 2015). In this case, evolving “mushy zone” emerges, ~~which -and~~ separates between the solid and liquid regions, where the thawing or freezing begins and proceeds, accompanied by latent heat absorbance or release (e.g., Crank, 1984; Yang et al., 2020). Following this approach, instead of the mathematical boundary, we use a narrow transition mushy zone (shaded area in Fig. 3), with pore space consisting of a mixture of ice and water (Rubinstein, 1982). The local enthalpy in the mushy zone takes values in the range between those of the pure solid and liquid, and the temperature is approximated by a constant value, $T=\bar{T}_i$, equal to the phase change temperature (Crank, 1984).

Heat exchange in the sub-surface is controlled by the ground temperature gradient, as well as by the soil thermal properties (i.e. thermal conductivity, Burn, 2011). Above ground, the main factor is the air temperature, which is measured and reported as MAAT (Luo et al., 2018; Szafraniec & Dobiński, 2020), ~~which-and is-was~~ taken as representing the MAGST (Mean Annual Ground Surface Temperature). Initial surface temperature ~~is-was~~ defined according to the temperature of the shallow seawater during mid-Holocene (2°C, Rasmussen et al., 2012), while the initial temperature profile (~~b~~Black ~~solid~~ line in Fig. 3) ~~is-was~~ defined using the regional average geothermal gradient of 0.033°C m⁻¹, as discussed by Olausen et al., (2019) and Betlem et al., (2018). The lower boundary of the model was set at 300 m depth, with temperature of 12°C according to the initial temperature distribution. Throughout the simulation, we searched for the depth and time-dependent temperature distribution $T(z,t)$, schematically shown as a dashed ~~curved~~ line in Fig. 3.

225 ~~For the modelling~~ Several MAAT values were used for the modelling: (1) the current -5.8°C (measured at the Adventdalen 'Polygons' site, (Christiansen, 2005), 7 km from the fjord); (2) -4°C, which was taken from climate simulation models for the mid-Holocene (Park et al., 2019; see also Mangerud and Svendsen 2018; Van der Bilt et al., 2019); (3) -3°C and 0°C assumed by Humlum (2005) for the mid-Holocene. While snow may cause differences between MAAT and MAGST due to thermal insulation (Zhang, 2005), it was found that in western Svalbard, specifically in the flat landforms at Adventdalen, the differences between MAAT and MAGST are less than 0.5-°C (Christiansen, 2005; Lüthi 2010; 230 Etzelmüller et al., 2011; Farnsworth 2013). Therefore, MAAT was taken as representing MAGST. Amplitude of seasonal temperature oscillation at the surface was set to 12°C, similar to the current fluctuation (Nordli et al., 2014; Christiansen, 2005; Osuch & Wawrzyniak, 2017).

235 -To distinguish between a frozen and water saturated cell, we defined a time and depth-dependent freezing ratio, $B(z,t)$, shown by points line in Fig. 3. $B=1$ means that the soil is water-saturated, while in the case of $B=0$ pore space is fully ice-saturated. In the mushy zone (shaded area in Fig. 3), the B -value changes between 0 and 1, and the rate of its change defines the amount of energy or latent heat associated with water-ice phase transition. Since it is now well-established that permafrost is not necessarily fully frozen (e.g. Keating et al., 2017; Oldenborger & LeBlanc, 2018; see Table 1), we also investigated permafrost aggradation under "partial freezing" conditions of 25% and 50%. Note that our 240 model assumes fully-saturated pore-water conditions, since freezing starts at sea level, soon after exposure, therefore groundwater level is expected to be at the surface.

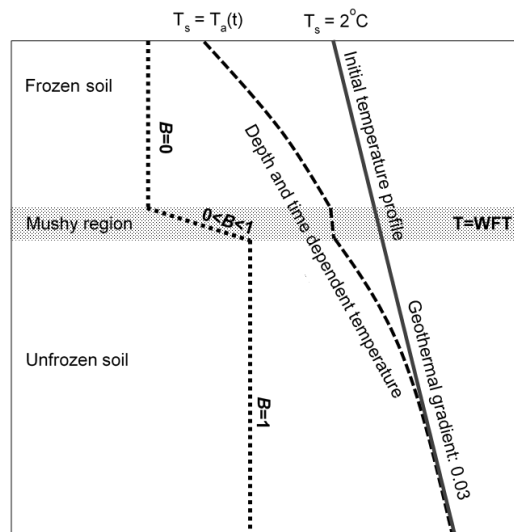


Figure 3. Schematic freezing profile during the top-down (epigenetic) freezing process. Initial and the developing geothermal gradients are also shown; the mushy region with constant temperature is the depth zone where phase transition occurs. Dotted line schematically represents the freezing condition, where $B=0$ stands for fully frozen and $B=1$ for liquid only. Active layer seasonality is neglected.

245

Another factor affecting the rate of permafrost formation is the water-freezing temperature (hereafter: WFT), which varies with salinity (Morgenstern & Anderson, 1973), as well as due to other environmental factors (Farouki, 1981; Morgenstern & Anderson 1973). Since salinities in the ADE site, down to 12 m, do not exceed 15% that of seawater, fresh water freezing temperature is the most appropriate for our simulations. Nevertheless, we also conducted simulations with WFT of -2°C , which is close to that of seawater ($T_m=-1.9^{\circ}\text{C}$, Marion et al., 1999; Bodnar, 1993), as well as with -6°C , following the reports of [Ggilbert et al., \(2019\)](#) and [Tavakoli et al., \(2021\)](#) about high salinities (up to 73 ppt) in [cryopegs in Adventdalen permafrost, which may reduce the freezing temperature down to \$-5^{\circ}\$ and \$-6^{\circ}\text{C}\$, respectively.](#) For simplicity, to determine thermal conductivity, was calculated considering three major components are involved: water, ice and bulk dry sediments. While the thermal conductivity of water and ice are well defined (e.g 0.569 and 2.24; $\text{W m}^{-1} \text{K}^{-1}$, respectively; [Williams and Smith, 1989](#)), the range of conductivity

250

255

מעוצב:גופן: נטוי, גופן עבור עברית ושפות אחרות: נטוי

מעוצב:גופן: נטוי, גופן עבור עברית ושפות אחרות: נטוי

מעוצב:אנגלית (ארצות הברית)

מעוצב:כתב עילי

260 values for dry sediment in the literature is large, from 0.25 to ~~W~~ 8.8- $W m^{-1} K^{-1}$ (Farouki, 1981; Williams and Smith, 1989). In Adventdalen, a recently published freezing model, used thermal conductivity of 0.5 $W m^{-1} K^{-1}$ for quaternary sediments (Hornum et al., 2020). We decided to ~~u~~mainly use the value of 0.35 $W m^{-1} K^{-1}$ for the dry sediment (~~mK~~ K^{-1}) to test the lower edge of thermal conductivity (i.e. anticipated slower freezing), while we also present results using ~~and a~~ high value of 3- $W m^{-1} K^{-1}$ (~~mK~~ K^{-1}) to examine higher boundary (Overduin et al., 2019).

מעוצב:כתב עילי

מעוצב:כתב עילי

265 Porosity is an important factor in the aggradation or thawing of permafrost (Hornum et al., 2020). It determines both the amount of heat released or required during freezing/thawing, and the thermal characteristics of the soil (ice has significantly higher thermal conductivity than water; Farouki, 1981). Porosity of sediments at ADE was mainly set to its average value, 0.3 (Gilbert et al., 2018), although we also tested the effect of other porosity values (Appendix 1). Bedrock (≥ 25 m depth) porosity was taken as 0.1, the value suggested by Hornum et al. (2020), assuming that the bedrock is mainly composed of fractured shales (Grundvåg et al., 2019; Benn and Evans, 2014).

270 Freezing temperature and degree of freezing were kept uniform in each of the simulations, although as pore water freezes, the remaining fluid becomes saltier, further lowering the freezing temperature of the remaining solute (Herut et al., 1990), such that fully frozen pore space (i.e. 100% freezing) can only be reached at extremely low temperatures, which are not relevant to our study sites, as well as to most other permafrost areas (Homshaw, 1980; Dobinski, 2011).

275 The 1-D freezing model provides a good approximation of freezing rate and permafrost aggradation as shown by many studies (e.g., Harada & Yoshikawa, 1996; Kukkonen & Šafanda, 2001; Farbrot et al., 2007; Etzelmüller et al., 2011; Hornum et al., 2020). Such models actually provide the maximum rates of freezing propagation, as lateral heat transport by groundwater flow is neglected. Neglecting lateral heat transfer is quite justified, considering that (1) upstream shallow groundwater arrive from areas that were exposed earlier, therefore should not be warmer than the ADE groundwater, (2) experimental data suggest that a temperature drop by a tenth of a centigrade below 0°C reduces the hydraulic conductivity by several orders of magnitude (Burt & Williams, 1976; Rūhaak et al., 2015). Nevertheless, as stressed above, soon after freezing initiates, the hydraulic conductivity dramatically decreases and the impact of lateral flow ~~can~~ould be neglected.

5.2 Mathematical formulation

290 The heat conduction equation for time and depth-dependent temperature profile, $T(z,t)$, is (Crank, 1984):

$$\rho C_p \frac{\partial T}{\partial t} = \frac{\partial}{\partial z} \left(\kappa \frac{\partial T}{\partial z} \right) + Q \quad (1)$$

where Q is the energy sink or source, representing the latent heat associated with water-ice phase transition, ρ is the soil density, C_p is the specific heat capacity and K is heat conductivity. The depth and time-dependent material properties were calculated assuming linear superposition of the soil, water, and ice properties (e.g., Lunardini, 1988). Thus, the depth-dependent density, heat capacity, and thermal conductivity were calculated using the porosity, θ , and freezing ratio, $B(z,t)$:

$$\begin{cases} \rho = (1 - \theta) \rho_{soil} + \theta ((1 - B)\rho_{ice} + B\rho_{water}) \rightarrow \\ \kappa = (1 - \theta) \kappa_{soil} + \theta ((1 - B)\kappa_{ice} + B\kappa_{water}) \rightarrow \\ C_p = (1 - \theta) C_{psoil} + \theta ((1 - B)C_{pice} + BC_{pwater}) \rightarrow \end{cases} \quad (2)$$

The thermal properties and density used for all system components (soil, ice and water) are listed in Table 2.

305 Out of the mushy zone, for ~~either the completely frozen ($B=0$) or unfrozen ($B=1$ (unfrozen) sediments)~~, the heat exchange leads to its cooling below or heating above the freezing temperature. When no latent heat is involved, assuming homogeneous heat conductivity, the heat conduction equation (1) is reduced to:

$$\frac{\partial T}{\partial t} = D \frac{\partial^2 T}{\partial z^2} \quad (3)$$

where D (diffusivity) [$m^2 s^{-1}$] defined as:

$$310 D = \frac{\kappa}{\rho C_p}$$

In the mushy zone, where the water-ice phase transition occurs, both the B value and the thermal properties (C_p and K) are depth-dependent. Accordingly, the complete heat conduction equation (1) is solved, including the latent heat term. The heat source/sink is equal to the mass of the freezing/thawing water per unit time multiplied by the latent heat, L . The water mass is equal to the rate of the B -value change times porosity and density. Finally, the source term is:

315

מעוצב:גופן: נטוי, גופן עבור עברית ושפות אחרות: נטוי

מעוצב:גופן: נטוי, גופן עבור עברית ושפות אחרות: נטוי

$$Q = -L \theta \rho \frac{\partial B}{\partial t} \quad (4)$$

We neglected the kinetics of the phase transition and assumed that thermodynamic equilibrium is established instantaneously in the mushy zone. This means that the rate of freezing/thawing is defined by the heat flux to and from the mushy zone with $0 < B < 1$. Substituting (4) into (1) and using $\frac{\partial T}{\partial t} = 0$ leads

320 to:

$$\theta L \rho \frac{\partial B}{\partial t} = \frac{\partial}{\partial z} \left(\kappa \frac{\partial T}{\partial z} \right) \quad (5)$$

The above equations are solved numerically for two functions $T(z,t)$ and $B(z,t)$, using the explicit-in-time finite difference scheme. These functions were approximated using the constant grid steps in depth Δz and in time Δt .

$$325 \quad T_{n,m} = T(n\Delta z, m\Delta t)$$

$$B_{n,m} = B(n\Delta z, m\Delta t)$$

where n is the grid point number ($z = n\Delta z$) and m is the time step number ($t = m\Delta t$). With this notation, the finite difference form of the heat conduction equation (1) is:

$$330 \quad \rho_n C p_n \frac{T_{n,m+1} - T_{n,m}}{\Delta t} = \frac{1}{\Delta z^2} \left[\frac{\kappa_{m+1} + \kappa_m}{2} (T_{n+1,m} - T_{n,m}) - \frac{\kappa_m + \kappa_{m-1}}{2} (T_{n,m} - T_{n,m-1}) \right] + L \rho \theta \frac{B_{n,m+1} - B_{n,m}}{\Delta t} \quad (6)$$

where density and the thermal properties are calculated using equation (2).

335 Equation (6) is solved using time step $\Delta t = 3210,6800\text{-s}$ ([i.e 3 hours](#)) (~~0.5 day~~) and a depth spacing $\Delta z = 0.25\text{ m}$. The solution was obtained for the model size down to 300 m depth, summing up to 1,200 grid points. These numerical parameters satisfy the von Neumann stability condition for explicit-in-time numerical scheme (e.g., Ames, 1977) for the material properties of Table 2. The numerical code was written with Python (Wang & Oliphant, 2012). It allows simulating the permafrost dynamics and sub-surface sediments freezing under various scenarios of MAAT, water freezing temperatures (WFT) and freezing extent of pore space water.

340 Table 2: 1-D heat transfer model physical parameters of water, ice and [dry soil](#).

| | Thermal conductivity | Heat capacity | Density | Diffusivity | Latent heat |
|--|----------------------|---------------|---------|-------------|-------------|
|--|----------------------|---------------|---------|-------------|-------------|

מעוצב:כתב עילי
 טבלה מעוצבת
 מעוצב:כתב עילי
 מעוצב:כתב עילי
 מעוצב:כתב עילי

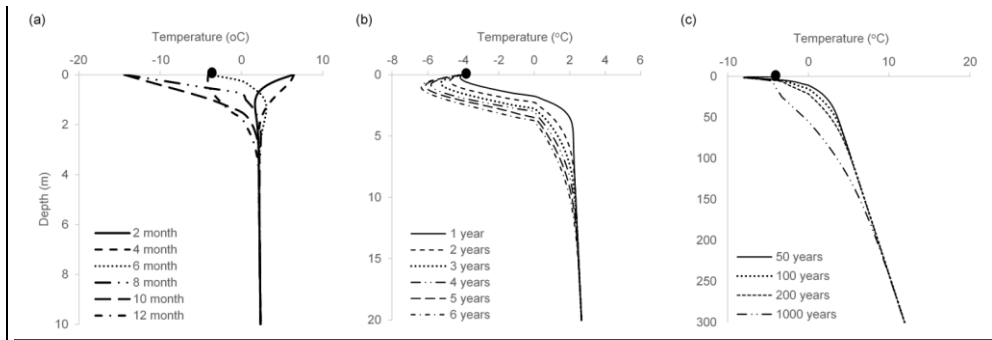
| | κ [$W m^{-1} K^{-1}$] | C_p [$J / (K \cdot Kg^{-1})$] | ρ [Kg / m^3] | D [$(m^2 / s)^{-1}$]* | L [J / Kg^{-1}] |
|-------------|--------------------------------|-----------------------------------|-----------------------|--------------------------------|-----------------------|
| Ice | 2.24 | 2100 | 916.2 | 1.17×10^{-6} | 334000 |
| Water | 0.569 | 4192 | 999.85 | 1.36×10^{-7} | |
| Soil (Silt) | dry unfrozen | 837 | | 1.74×10^{-7} unfrozen | |
| | dry frozen | 712 | 2400 | 2.04×10^{-7} frozen | |

* $D = \kappa / \rho \cdot C_p$

5.3 Model results

We present the results of model runs with variable combinations of surface temperature, water freezing
 345 temperature and sediments porosities and thermal conductivities. Complementary modelling results are
 presented in the Appendix. In all cases, simulations started in the spring (May) and followed an amplitude
 of 12°C around the chosen (fixed) MAAT.

We first present simulations with MAAT of $-4 \pm 12^\circ C$, WFT $0^\circ C$, and complete (100%) freezing. Results
 350 in parentheses are for sediment thermal conductivity of $3 W m^{-1} K^{-1}$. Figure 4a presents results of a one-
 year simulation, with temperature profiles shown every second month. The model suggests that freezing
 under these conditions can reach down to two meters (3) depth within the first year. The freezing depth
 increases to 4 (6) m within 6 years with a slight, but significant deepening of the winter inflection point
 (Fig. 4b). After 50 years, freezing arrives at 10-11 (16-17) m, and within 1000 years the freezing front is
 355 already at 50 (73) m (Fig. 4c) in the sedimentary basement rocks (considering that sediment cover at
 ADE is ca. 25 m). The depth affected by cooling also progresses with time (<50 m in 50 years, >150 m
 in 1000 years) and T profile approaches linearity.



360 Figure 4. 1-D freezing model results for: (a) 1 year; the model starts (and finishes) at spring, defined as
mid-time between minimum and maximum surface T (e.g. May), followed by summer increase in
temperature (solid and dashed lines), cooling and start of freezing during fall (point-dotted line, e.g.
November), followed by colder winter months (two-points dashed line and wide dashed line) and
concluding in the spring (one point dashed line); (b) 6 years (starting in spring). MAAT $-4 \pm 12^{\circ}\text{C}$, WFT
365 set at 0°C , 100% freezing. (C) Model simulation for 50 to 1000 years. Black circles dots denote -4°C .
Note the different scale between (a) (b) and (c).

Lowering the WFT results in decrease of the freezing rate. For example, with WFT of 0°C freezing front
will reach 15 (23) and 21 (37) m after 100 and 200 years while with WFT of -2°C and -5°C it will reach
370 11 (15) and 16 (20) m and 4.75 (2.5) and 6.75 (2.5) m during the same periods, respectively (Fig. 5).
Surprisingly, permafrost aggrades even under WFT of -5°C , which is lower than the annual-average-air
temperature (MAAT) of -4°C . This is because the thermal conductivity of ice is higher than that of water
(Farouki, 1981), which results in a deeper advance of the winter freezing front (through ice) than the
advance of summer thawing (through water). Permafrost aggradation was not observed under WFT of $-$
375 5°C when using a dry sediment conductivity of $3\text{-W m}^{-1}\text{ K}^{-1}$.

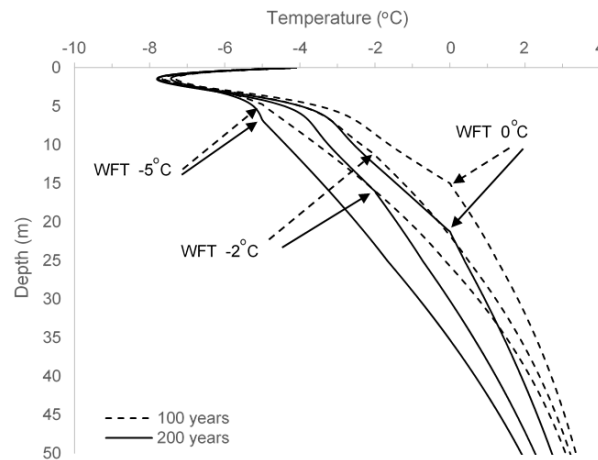
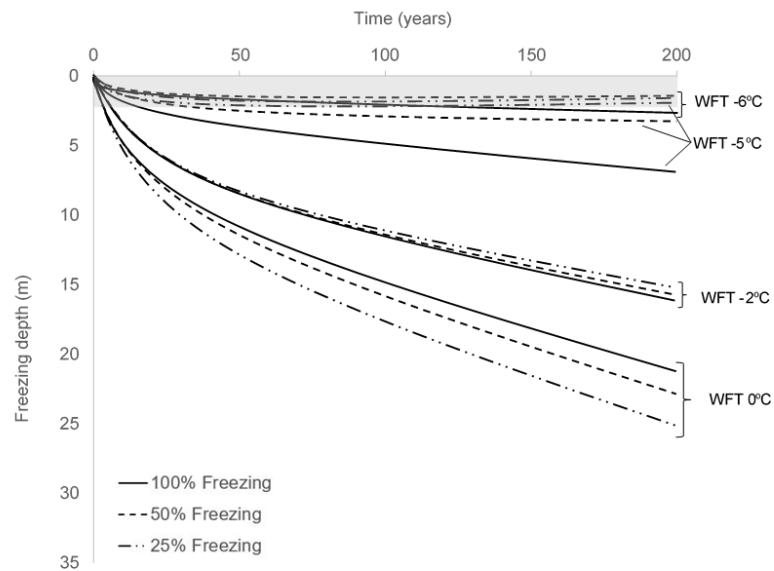


Figure 5. [Results of 1-D freezing model results simulations](#) with mid-Holocene MAAT of $-4^{\circ}\text{C} \pm 12^{\circ}\text{C}$ (Park et al., 2019), [with and](#) pore-water freezing temperature (WFT), taken as 0°C , -2°C and -5°C .
 380 Simulations [include were run for](#) 100 and 200 years.

In Figure 6, we examine the effect of partial freezing. Partial freezing (25% and 50% in our scenarios) result in deepening of the freezing depth, but differences are relatively small. With MAAT of -4°C and WFT of 0°C , after 200 years freezing depth will reach 21, 22 and 25 m with 100% 50% and 25% freezing, respectively. Lowering WFT to -2°C , [the freezing depth become even more similar will differ by less than 4 m](#) (16 to 15.25 m), [within the three scenarios](#) (Fig. 6). This is because of the trade-of between reducing latent heat and the lower thermal conductivity of the partially frozen pore space. [Moreover, wW](#) with a WFT of -5°C , the trend changes, and permafrost aggradation will occur only under the 100% freezing scenario. [Under, while with](#) partial freezing of 25-50%, it will not [exceed aggrade](#) deeper than 2 m (Fig. 6), i.e. no permafrost will develop (assuming active layer depth of 1-2 m), which [further](#) suggests that when WFT is lower than the average MAAT (-4°C), aggradation is controlled by the ice thermal conductivity rather than by latent heat. Last, with WFT of -6°C (i.e. significantly lower than the MAAT), there is no apparent permafrost aggradation also with 100% freezing (assuming active layer depth of 2
 390

395 m, Fig. 6), although permafrost does develop to ca. 3.5 m after 1000 year (not shown). With thermal conductivity of $3W\ m^{-1}\ K^{-1}$, 25% partial freezing will result in significantly deeper (10 m) permafrost aggradation. However, with WFT of $-2\ ^\circ C$, aggradation rates with 100% and 25% freezing turn similar, and with WFT of -5 or lower, permafrost will not aggrade.



400 Figure 6. Mid Holocene permafrost aggradation with variable freezing degrees. MAAT was set to $-4\ ^\circ C$ (Park et al., 2019), and freezing proportions were taken as 100%, 50% and 25%. The shaded/grayish zone represents a hypothetical, conservative, active layer, which is taken at-as 2 m thick. We note that currently active layer at the area in Adventdalen is usually ≤ 1 m, and 2 m was chosen due to the higher temperature during the mid-Holocene.

405

מעוצב:כתב עילי

מעוצב:כתב עילי

מעוצב:כתב עילי

מעוצב:כתב עילי

מעוצב:כתב עילי

מעוצב:כתב עילי

מעוצב:כתב עילי

מעוצב:כתב עילי

מעוצב:כתב עילי

410

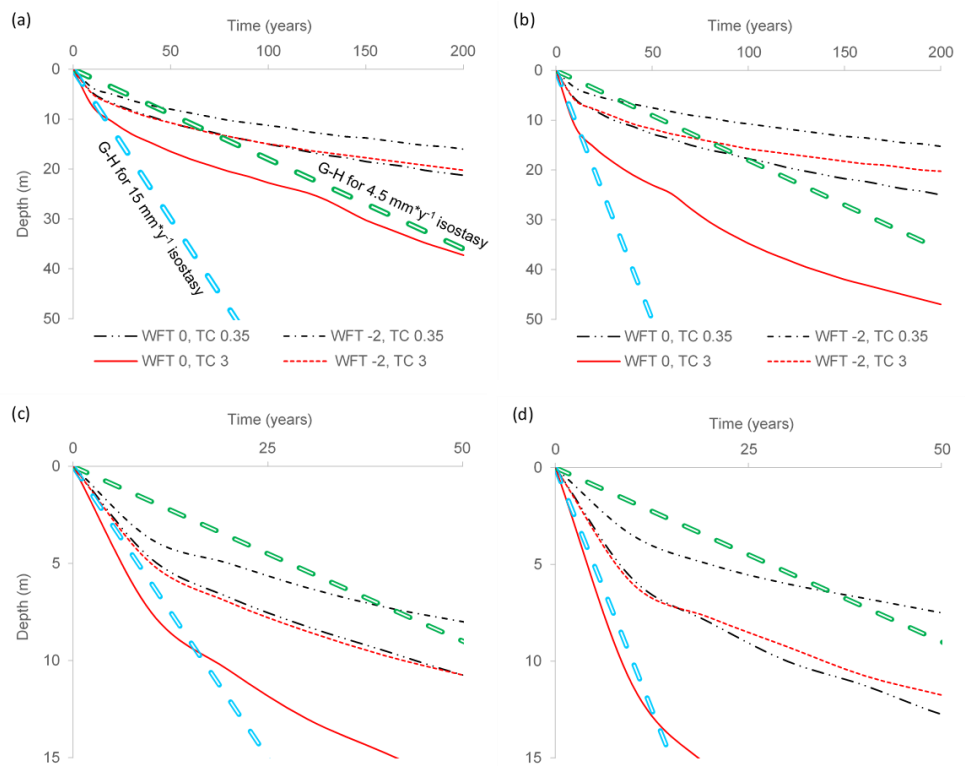
415

420

מעוצב:כתב עילי

מעוצב:כתב עילי

In general, higher MAAT ~~leads to results in the a~~ lower aggradation rate (Fig. 7a-b, e-f) e.g. with MAAT of 0°C and WFT of 0°C 100% freezing and Thermal conductivity of $0.35 \text{ W m}^{-1}\text{K}^{-1}$ freezing depth will reach 12 m within 200 y. Changing the thermal conductivity to $3 \text{ W m}^{-1}\text{K}^{-1}$ will result in 9.5 m freezing depth. For the same setting, but with MAAT of -4°C the freezing front will result in significant deepening, while with Thermal conductivity of $3 \text{ W m}^{-1}\text{K}^{-1}$, it will reach 37 m and for thermal conductivity of $0.35 \text{ W m}^{-1}\text{K}^{-1}$, it will reach 21 m (Figure 7a). Setting the system to 25% freezing, freezing depth will reach 47 and 25 m respectively (Fig. 7b). However, we show that even with MAAT > WFT (e.g., 0°C and -2°C , respectively) freezing will arrive at 3.5 m after 200 years and 8 m after 1000 years (not shown). As mentioned above, this is due to the asymmetry in the seasonal freezing/thawing process. Higher conductivity during winter (frozen pore space) enhances the loss of heat, while the lower conductivity during summer (warming front goes through thawed pore space) slows the thawing process (Kukkonen & Šafanda, 2001). We note that lower proportions of freezing (e.g., 25%) will have the effect of reducing this asymmetry due to the higher proportions of liquid water in the cryotic pore-space, therefore lower thermal conductivity during freezing. Accordingly, permafrost deepening is hardly observed in the scenario of MAAT = 0°C (in particular with WFT = -2°C ; compare Fig. 7a and 7b). Thermal conductivity of $3 \text{ W m}^{-1}\text{K}^{-1}$ (Fig. 7 e-f) will result in faster deepening of the freezing front.



425

מעוצב:כתב עילי

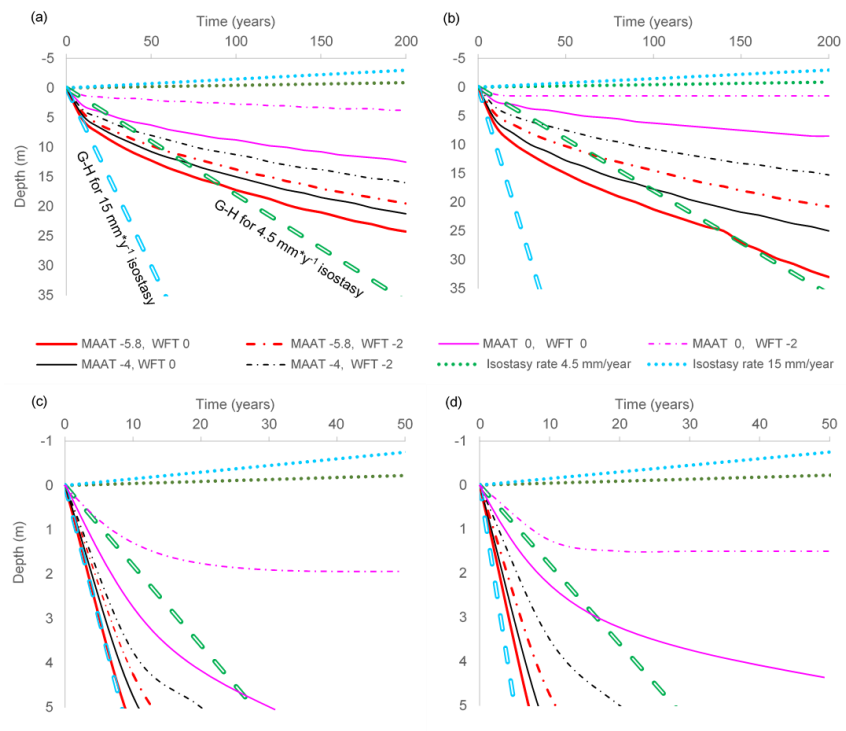
מעוצב:כתב עילי

מעוצב:כתב עילי

מעוצב:כתב עילי

430

Figure 7. Early and mid-Holocene freezing depth in the first 50 and 200 years with MAAT -4°C and WFT of 0 and -2°C and with thermal conductivity (TC) of 0.35 and $3\text{ W m}^{-1}\text{K}^{-1}$. (a) 100% freezing, (b) 25% freezing. Also shown are curves of two scenarios of corresponding depths of the fresh-saline water interface, using a 1:40 Ghyben-Hertzberg (G-H) approximation for isostasy of 4.5 and 15 mm y^{-1} . See text for more details. (c) and (d) are zoomed in of (a) and (b) for the first 50 years. The fast deepening in figures a, and b is due to change in porosity as the freezing front reaches the bedrock (25 m). The legend is the same for all figures.



435

מעוצב:אנגלית (ארצות הברית)

440

Figure 7. Early and mid-Holocene freezing depth in the first 50 and 200 years with corresponding different MAAT, -5.8°C , and -4°C respectively, and with WFT of 0°C and -2°C . (a) 100% freezing, (b) 25% freezing. Also shown are curves of two scenarios of corresponding depths of the fresh-saline water interface, using a 1:40 Ghyben Hertzberg (G-H) approximation for isostasy of 4.5 and 15 $\text{mm}\cdot\text{y}^{-1}$. See text for more details. (c) and (d) are zoomed in of (a) and (b) respectively for 5 m depth and for the first

445 ~~50 years. The fast deepening in figures b, e and f is due to change in porosity as the freezing front reaches the bedrock. The is the same for all figures.~~

6. Discussion

6.1 Ground ice salinity and the frozen interface

450 When the freezing front propagates downwards in a recently emerged land and epigenetic permafrost is formed, it might freeze old subsurface brines (Cascoyne, 2000). As the freezing process proceeds, solute concentrations in the non-frozen residual water commonly increase (e.g., Cocks and Brower, 1974; Herut et al., 1990; El Kadi and Janajreh, 2017). ~~This which~~ results in a pore space with ~~low water activity and~~ high salt concentrations. ~~These resulted~~ brines may then migrate away from the freezing surface, driven by density and capillary forces, and coalesce to form separate saline water lenses ('cryopegs'; Cascoyne, 455 2000). The level of salinity and water composition will depend on the initial water composition and the extent of freezing.

Complete permafrost freezing can hardly be obtained, since the eutectic point of seawater freezing is at ~~-36°C to -54°C~~ (Gitterman 1937; Ringer 1905; Nelson & Thompson 1954; Marion et al., 1999), while ~~in~~ Adventdalen permafrost temperatures does not usually get below ~~-6°C~~, below depth of zero annual amplitude (ZAA) (Christiansen et al., 2010), and are never lower than ~~-12°C~~ even in the shallow permafrost (Christiansen et al., 2020; Isaksen et al., 2007). Although the eutectic point is well below the expected temperature values, the freezing-salt expulsion process still prevails. Under these conditions, the permafrost pore space should hold a small fraction of residual brine solution, which contains most of the solutes originally dissolved in the bulk pore-space water. Partly ~~un~~ frozen permafrost 465 has been often observed in the study area- during drilling, in particular deeper than a few meters, ~~where seasonal impact is not relevant~~. This was also ~~found in both deciphered from~~ geophysical and geochemical observations (e.g., Keating et al., 2018; Weinstein et al., 2019). Nevertheless, when ground ice is thawed, the extracted fluid from the relatively large segments used in this study should roughly indicate the salinity of the original in situ pore fluid, assuming no major brine migration had occurred.

470 Pore-water composition may be significantly altered from the original fluid that circulated in the sediments (e.g., seawater) due to ion exchange or dissolution prior to or even after cryotic conditions ~~occurred took place~~, which is reflected in the Na/Cl and SO₄/Cl ratios in the thawed ground ice (Fig. 2). Nevertheless,

475 Cl⁻ concentration is probably close to and represents the salinity of the original pore fluid. We note that while in certain cases permafrost contains lenses or pockets of unfrozen brine-containing cryotic soils ('cryopegs', e.g. Van Everdingen, 1998), which are commonly attributed to the segregation and migration of fluids (i.e. non in situ). The relatively low salinity (Fig. 2) and the evident mixing profile (Fig. 2a, b and C), suggest that this is not the case in the ADE site, and that the observed fresh-seawater interface is an in situ observation. We relate to the chemistry of the extracted fluid as 'ground ice chemistry', although it could as well be that some of it was not actually frozen.

מעוצב:אנגלית (ארצות הברית)

480 Cable et al., (2018) presented ground ice chemistry of cores from the Adventdalen, albeit closer to the current fjord (<4 km), west of the ADE site. In these cores, chloride, ~~s~~Sodium and ~~s~~Sulphate concentrations at depths of 3-11 m were up to 50% that of seawater. At ADE, farther away from the sea, ground ice in the epigenetic permafrost, ~~from~~ 5.5-m from the surface and deeper, shows a gradual increase in salinity (i.e., fresh-saline interface), with Cl⁻ concentrations reaching 15% that of seawater at 485 9 m below the surface. Although salinities do not change much between 9-12 m, it is likely that ~~a~~ more saline water, close to seawater salinity, either exists today or existed in the past (prior to freezing) at deeper permafrost levels.

The existence of a fresh-saline interface in the very shallow permafrost, in fact at the top of the epigenetic permafrost, suggests that freezing at ADE occurred straightaway after emergence above seawater. This is further discussed below.

490

6.2 Rebound, exposure and fresh-saline interface ~~FSI~~ deepening

Assuming that Early Holocene (11-8 ka BP) precipitation was slightly higher than present (200 mm per year, Kjellman et al., 2020; McFarlin et al., 2018), and using a conservative infiltration factor of 0.2 (whether thawing snow or direct rain) and the porosity used in our simulations (0.3), this amounts to an 495 effective annual ~~rainfall~~-infiltration of ca. 1320 mm per year. This could easily keep up with the Early Holocene rebound rates of 15 mm y⁻¹ (established for the nearby Sassendalen Vallley, Salvigsen, 1984; Sessford et al., 2015), therefore preserving the groundwater table close to the surface of the emerging land. Using a Ghyben-Herzberg approximation (Bear & Dagan 1964), this would result in an Early Holocene fresh-saline interface deepening of ca. 60 m in 100 years (Fig. 7), assuming the saline water body had a common seawater density of 1,025 kg /m³. The FSI deepening could even be faster, if the deep water body is ~~l~~ess saline water body at depth would result in a deeper fresh-saline interface than seawater. ~~Even if sub-aerial~~ exposure occurred later, during the mid-Holocene, when the rebound rate

מעוצב:כתב עילי

500

decreased to 4.5 mm y⁻¹ (Forman et al., 2004), ~~the~~ fresh-saline interface ~~would~~ still deepen at a rate of 180-mm y⁻¹, i.e. 18 m in 100 years (Fig. 7).

505 The existence of a mixing zone at the top of the epigenetic permafrost (from 5.5 m below ~~the~~ current terrain surface), ~~and of water~~ with Cl⁻ content 15% that of seawater at 3.5 m below the Early Holocene surface, suggests that the marine sediment section at ADE was hardly flushed with meteoric water. ~~This~~ which further suggests that permafrost aggradation commenced shortly after emergence above the sea (e.g., Kasprzak et al., 2020). Indeed, some of the simulated freezing scenarios can clearly cope with the
510 above fresh-saline interface deepening rates (e.g., MAAT of ~~-5.84~~ °C and WFT of 0 °C, Fig. 7). Moreover, assuming that partial freezing (e.g., 50-25%) can also block flushing, this results in even faster permafrost aggradation (Fig. 7b). However, as permafrost deepens, freezing rate slows down (e.g., Fig. 7), and none of the scenarios can cope with the assumed deepening of the fresh-saline interface, which should result in flushing of deeper zones.

515 It ~~is seems likely suggested~~ that the key factor in fresh-saline interface fossilization in a continuous permafrost landscape is the permanent freezing of the very shallow permafrost, which hydraulically disconnects the sub-permafrost zone from the surface and prevents recharge of this zone with meteoric water. As shown ~~above~~ (Fig. 6 and 7), freezing of the top 3-5 m can occur within several years even with the relatively high temperatures of the Early to mid-Holocene (e.g., MAAT of -4 °C or even warmer, Fig.
520 7), therefore, the fresh-saline interface could effectively be preserved.

We did not include salt diffusion in our model (e.g. Angelopoulos et al., 2019), a process that will reduce WFT as freezing progresses. It can explain the reason for partially frozen samples extracted from the epigenetic section (table 1). Including salt diffusion, we assume the freezing front may have advanced somewhat slowly than suggested by our model.

525

6.3 Permafrost aggradation during the Holocene

Gilbert et al., (2018), suggested that our drilling site at ADE emerged from the sea at 10 to 9 Ka BP and
530 that the delta front advanced westwards at a rate of 4.4-m y⁻¹ prior to 9.2 Ka, which decreased to 0.9-m y⁻¹ during the rest of the Holocene. Considering the relatively high rebound rates during 9 to 8 ka (e.g., 15-19-mm y⁻¹), this suggests that the land surface at ADE reached 3-4 meters above sea level and a topographic gradient of 1-2% towards the sea within 200 years. Assuming ~~thethat~~ groundwater table was close to the surface, this should further result in a good flushing of the subsurface, unless freezing took

control (Fig. 8). The observed mixing zone, which reaches the very top of the pre-Late Holocene surface, suggests that freezing started within just a few years after exposure.

535 Our simulations suggest that both cryotic conditions (i.e., $<0^{\circ}\text{C}$) and actual ground ice formation were ~~started~~ achieved very soon after exposure to the atmosphere (Fig. 5, 6 and 7), and that significant freezing depths of 15-33 m ~~(or even 20-37 m considering higher thermal conductivity, Fig 7)~~ can be achieved with 200 years (Fig. 6 and 7). This is true for both the Early to mid-Holocene warmer period (Kutzbach & Guetter, 1986; McFarlin et al., 2018; Mangerud and Svendsen, 2018; Park et al., 2019; 540 Kjellman et al., 2020) and for any sub-zero average annual temperature MAAT, regardless the size of the annual fluctuations. We even tested MAAT of $+1^{\circ}\text{C}$ ~~finding and found~~ that some freezing could occur (not shown), which is a seasonal effect, derived from the different thermal conductivities of ice and water. Our simulations are in good agreement with Harada & Yoshikawa (1996), who ~~estimated~~ ~~using~~ used 1-D model with a MAGST of -5.7°C but not ~~totally-completely~~ saturated sediments ~~and found~~ that 533 years are needed to freeze 31.7 m of sediments in Moskuslagoon, slightly to the west of our 545 site, on the Adventfjorden shore.

The ADE site was free of sea water in the Early Holocene, prior to 9.2 ka BP (Gilbert et al. 2019?). At that time, an abrupt cooling ~~was~~ has been described in Svalbard (Mangerud and Svendsen, 2017; van der Bilt et al., 2018, 2019). The presented model results show that the initiation of permafrost and its 550 gradual aggradation is possible under relatively high temperatures (yet $\text{MAAT} \leq 0^{\circ}\text{C}$) of the mid-Holocene. Christiansen et al. (2013), pointed out that local topographic conditions and winds in Adventdalen can induce lower temperatures at low altitude depressions, which could enhance the permafrost aggradation during the mid-Holocene.

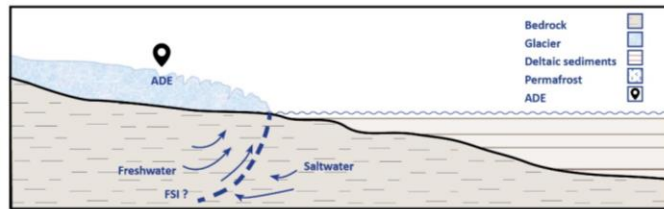
Our simulations also show that lower percentage of freezing (e.g., 25%) may ~~deepen freezing and~~ enhance the permafrost aggradation rate (e.g., Fig. 7b); however, this is not true for lower WFT (e.g., -2°C) or for relatively high MAAT (e.g. 0°C , ~~compare Fig. 7b b with 7a~~), which as mentioned above is due to the trade-off between latent heat and thermal conductivity differences between ice and liquid water. Nevertheless, MAAT of 0°C seems unlikely (e.g., Van der Bilt et al., 2019).

In summary, the simulations suggest that permafrost aggradation could and did occur ~~even immediately~~ following exposure also during the ~~Early~~ the relatively warm period of ~~.....~~ Early to Mid Holocene 560 ~~(40-8??-8-10 ka BP)~~, and probably as well during exposure in the mid-Holocene. This is in agreement with Hornum et al., (2020) for the Early to mid-Holocene cooling 9-8 Ka BP. Our findings of a frozen fresh-saline interface suggests that the ground at ADE remain frozen during the Holocene thermal

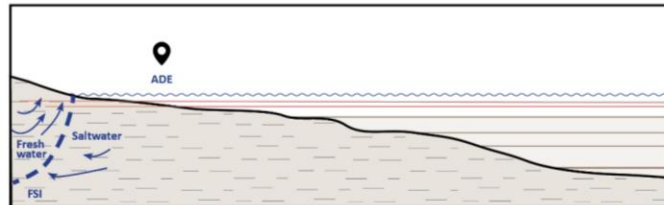
565 ~~maximum which~~This is in disagreement with Hornum et al., 2020, who suggested that ~~while freezing did~~
~~occur during the Early Holocene~~ the ground thawed ~~during the Mid Holocene and~~ and refroze ~~at~~ about
6.5 Ka BP.

570 ~~Pleistocene p~~Permafrost dynamics ~~during the Holocene~~ were studied in other permafrost regions. While
in some areas there are records of permafrost degradation and peatland expansion already in the Early
Holocene (post deglaciation, e.g., Lenz et al., 2015; Kaufman et al., 2015; Grinter et al., 2018; Li et al.,
2021), cumulated evidence indicates that ~~air~~ temperature during this period was highly variable,
sometimes higher and sometimes lower than ~~in~~ presently ~~days~~ (Kaufman et al., 2015). Nevertheless, it
is a common observation that during the Holocene Thermal Maximum (mid-Holocene, 8.2-4.2 ka BP)
permafrost has been degrading and thermokarst peaked (e.g., Lenz et al., 2015; Ulrich et al., 2017;
Anderson et al., 2019). Permafrost aggradation resumed post- 6 ka, and mainly during the past 4-3 ka
575 (e.g., Grinter et al., 2018; Treat and Jones, 2018). ~~As shown above, we believe that this was not the~~
~~case in Svalbard, and exposed lands continued freezing throughout the Pleistocene.~~

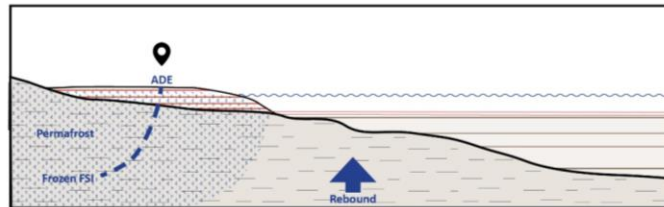
580 ~~The ADE site was free of sea water cover in the Early Holocene, prior to 9.2 ka BP. At that time, an~~
~~abrupt cooling was described in Svalbard (Mangerud and Svendsen, 2017; van der Bilt et al., 2018,~~
~~2019). The presented model results show that the initiation of permafrost and its gradual aggradation is~~
~~possible under relatively high temperatures (yet MAAT \leq 0°C) of the mid-Holocene. Christiansen et al.~~
~~(2013) pointed out that local topographic conditions and winds in Adventdalen can induce lower~~
~~temperatures at low-altitude depressions, which could enhance the permafrost aggradation during the~~
~~mid-Holocene.~~



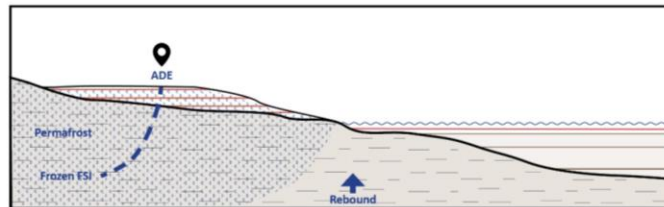
Stage 1: 22K Ka BP: Last glacial cycle, the glacier advances, and the valley bottom is eroded down to the bedrock (Elverhøi et al., 1995). The FSI is probably located at the meeting point of the sea and land.



Stage 2: 10-10.5 Ka BP: Maximal sea ingression (Lønne & Nemeč, 2004) and deltaic sediments deposition (Gilbert et al., 2018). The FSI migrates eastward to the new location where sea and land meet.



Stage 3: 9.5 Ka BP: The FSI migrates westward and freezes when temperatures drop sharply. Freezing front (from top down) exceeds fresh water lateral flow. Epigenetic permafrost aggrads.



Stage 4: ADE site at present. Fluvial and aeolian deposition freeze syngenetically (Gilbert et al., 2018).

Figure 8. ~~a~~ Conceptual presentation of the type of ground water freezing ~~major~~ processes in Adventdalen since the last glacial cycle with a focus on ~~and the freezing of the fresh-saline water interface (FSI) at the ADE site.~~

590

7. Summary and conclusions

Arctic landscapes Land surface at northern territories, including western Svalbard, was rising relatively fast in the Early to mid-Holocene due to glacial isostatic rebound. Accordingly, the preservation of a frozen saline water (mixing zone) at a very shallow depths next to Early to mid-Holocene surface is taken as evidence for fast permafrost aggradation, which could halt the infiltration of fresh meteoric water and the flushing of saline water to the sea. This is despite of the prevailing relatively high~~warm~~ temperatures during this period.

Our modelling confirms that freezing could progress relatively fast down the exposed Adventdalen sediments, i.e. to 15-25 m within 200 years, even under the reconstructed relatively high mid-Holocene air presumed mid-Holocene of -4°C used in the 1-D model. temperatures.

מעוצב:כתב עילי

The modelling further suggests that permafrost may aggrade even when water freezing temperature (WFT) is slightly lower than MAAT, which is due to the differences in thermal properties between ice and liquid water.

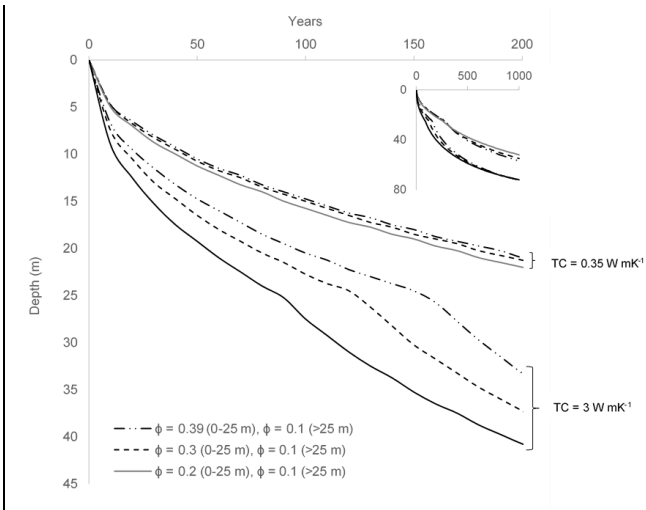
~~Non-Non~~-complete freezing of the cryogenic pore space could result in faster deepening of the freezing front when MAAT is smaller than WFT or even when it is higher, but in the latter case the difference is not large (e.g., MAAT < 0 °C and 0 < WFT > -2 °C). However, when MAAT >> WFT (e.g., MAAT = 0 °C and WFT ≤ -2 °C), the presence of liquid water in the pore space and its lower thermal conductivity would result in a halt of permafrost aggradation.

This concept of fast freezing under relatively ~~warm~~ high air temperatures may suggest that recently exposed areas may still go through permafrost aggradation even under the current global warming. Also, it could imply that a short (years to decades) cooling period could significantly slow down permafrost thawing.

8. Appendix

615 Appendix 1: Porosity analyses

Selected simulation results demonstrating the effects of the porosity values on the rate of permafrost formation with thermal conductivities of 0.35 and 3 W m⁻¹ K⁻¹, are presented in figures 8-9 - 11-12. In general, higher porosity (i.e., more pore water to freeze) will result in slower permafrost aggradation (Fig. 8-9 and 10-11) due to the higher latent heat involved. Nevertheless, with low soil thermal conductivity and with lower WFT (i.e., closer to MAAT, Fig. 9-10a) the differences in aggradation rates with different porosity values are small and even negligible (Fig. 9a and 11a). when thermal conductivity is an order of magnitude higher porosity values are much notable.



625 Figure 89. Simulations of freezing front progress with different porosities and two thermal conductivities (TC), for MAAT of -4 °C, WFT of 0 °C and 100% freezing. Inset present results for 1000 years. The fast deepening at depth > 25 m is due to change in porosity as the freezing front reaches the bedrock.

630

635

640

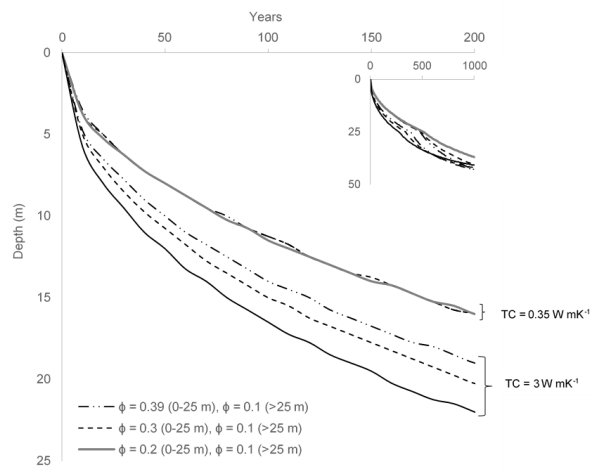


Figure 910. Simulations as in Fig. 89, but with WFT of -2 °C.

645

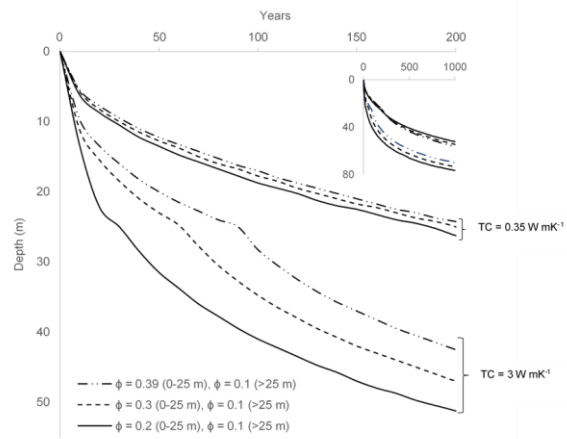


Figure 8-9. Simulations as in Fig. 8-9 (MAAT= -4 °C, WFT= 0 °C), but with 25% freezing.

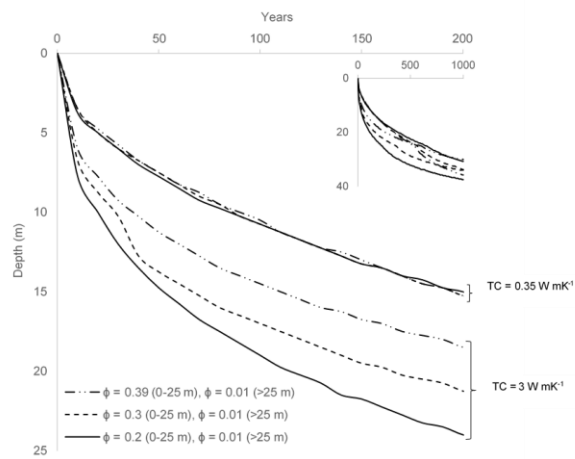


Figure 4.12. Simulations as in Fig. 9 (MAAT = -4 °C and WFT = -2 °C) but with 25% freezing.

9. Code availability

```
# 1-D freeze/thaw model code – copy and paste code rows into Python (Spider-Anaconda).
655 # This Python-script describes the 1-D Heat transfer model code developed for the research first Rotem
    et al., (202....). The 1-D model is a transient one-dimensional heat transfer model suitable for simulating
    permafrost dynamics. The core of the model is an explicit forward-difference time approximation of the
    one-dimensional heat transfer equation. This script is tailored to simulate the Holocene ground
    temperature development in Adventdalen, Svalbard, but may be modified to fit other purposes.
660 #Usage must be cited by reference to Rotem et al. (202....).
    #For references cited below see:...

    #Importing relevant packages for Python
    import numpy as np
665 import matplotlib.pyplot as plt
    import sys
    import pandas as pd

    n =1201          # number of point grid
670 | m1 =520        #number of snapshots – i.e. No. of curves as display in fig. 4 and 5, or No. of sub
    sets of data to be exported.
    m2 = 365*50      # number of steps for every snapshot
    m = m1*m2        # number of time step

675 | dt = 3600.0*24.0/28 #1/68 of a day 44400-10800 sec # 1000000sec =approx. 11.8 days
    t_final = dt*m    #defines the final time step
    t_days=t_final/3600./24. #converts time steps to days
    t_snap= dt*m2/3600./24.
    print ('t_snap')
```

```

680 z=300.0          #meters depth
    dz = (z/(n-1))  #meter - defines the cell width if cell width (dz).
    Tfr=0           #Freezing temperature define as WFT in article

    #define depth-porosity profile
685 Depth = np.zeros(n)
    por = np.zeros(n)
    for i in range (0,n):
        Depth [i] = -i*dz
        por[i] = 0.3          # sediment's porosity
690     if Depth[i] < -25.0:  # change from sediment's porosity to rock porosity
        por[i] = 0.1

    L = 334000.0        # J/kg water and ice Latent heat

695 #Density of materials
    p_ice = 916.2      # Kg/m^3
    p_water = 999.85  # Kg/m^3
    p_soil = 2400.0   # Kg/m^3

700 #Defines Heat conductivity (K) & Heat Capacity (Cp) as function of porosity.
    K_dufsoil = 0.35  #or 3W/(m*K) K_dufsoil = k of dry soil at temperatures ca. 5 °C centigrade.
    K_dfsoil = 0.35  #or 3 W/(m*K) K_dfsoil = k of dry soil at temperatures lower than 0 °C
    Cp_dufsoil = 837  #heat capacity of dry soil (silt) in ca. 10 °C Cp_dufsoil = Heat capacity of dry soil
    above 0 °C.
705 Cp_dfsoil = 712  #heat capacity of dry soil (silt) in ca. -10 °C Cp_dfsoil = Heat capacity of dry soil
    below 0 °C.
    K_ice = np.zeros(n)
    K_water = np.zeros(n)
    Cp_ice = np.zeros(n)
710 Cp_water = np.zeros(n)

```

```

for i in range (0,n):
    K_ice[i] = 2.24 *por[i] + K_dfsoil *(1-por[i])      # W/(m*K) regression with 0<B<1 -1.651x
    + 2.22
715    K_water[i] = 0.569*por[i] + K_dufsoil*(1-por[i])  # W/(m*K)
    Cp_ice[i] = 2100.0*por[i] + Cp_dfsoil *(1-por[i])  # j/(K*Kg)
    Cp_water[i] = 4192.0*por[i] + Cp_dufsoil*(1-por[i]) # j/(K*Kg) regression with 0<B<1 2.192x
    + 2. considering 90% soil and 10% water.

720 #control on model stability condition for explicit-in-time numerical scheme
    dd2=K_ice[i]/(p_soil*Cp_ice[i])*dt/dz/dz
    dd3=K_water[i]/(p_soil*Cp_water[i])*dt/dz/dz
    if dd2>0.25 or dd3>0.25:
        print(' Values must be < 0.25 ')
725     print(dd2,dd3)
        print(i,Depth[i],por[i])
        sys.exit(' Decrease time step ')

x=np.linspace(0,z,n)
730
#creating time field for data export
time=np.zeros(n)
for i in range (0,n):
    time[i]=0+dt*i
735
#initial conditions
B=np.ones(n)      # B is a variable between 0 and 1 considering the ratio of ice or water in a cell.
B=1=water, B=0=ice creates an array of 1
T=np.ones(n)     # Initial Temperature 2 Centigrade creates array of 2 centigrade across the soil profile
740 for i in range(0,n-1):
    T[i]= 2.0 + 0.033*i*dz #Thermal gradient 0.033 centigrade per m

```

```

#Define working arrays
Tn=np.zeros(n)      # creates an array for each one of the variables
745 Bnew=np.zeros(n)
K=np.zeros(n)
Cp=np.zeros(n)
p=np.zeros(n)
dE2=np.zeros(n)
750

for j1 in range(0,m1):  #a loop on the snapshots
for j2 in range(0,m2) :
#Boundary conditions
755   Time=(j1*m2+j2)*dt/3600./24/365  #years
   T[0]=12*np.sin(2.*np.pi*Time)-4  #surface temperature for seasonal variation
   B[0]=0.  #B=1=water, B=0=ice
   if T[0]>0:
       B[0]=1
760   T[n-1]= 2 + 0.033*z  #bottom of profile temperature. when sediments exposed to air it still has the sea
water temperature.
   B[n-1]=1.  #B=1=water, B=0=ice

   for i in range(0,n):  # calculate mixture properties each variable is calculated with linear ratio to B
765   (ice to water ratio in a cell).
       K[i]=K_ice[i]*(1.0-B[i])+K_water[i]*B[i]
       Cp[i]=Cp_ice[i]*(1.0-B[i])+Cp_water[i]*B[i]
       p[i]=p_ice*(1.0-B[i])+p_water*B[i]

770   for i in range(1,n-1):  # loop over internal points. the dE2 (energy equation) equation is split for more
convenient calculations
       dE2[i]=(K[i-1]+K[i])/2.0 * (T[i-1]-T[i])/dz

```

```

dE2[i]=dE2[i]-(K[i]+K[i+1])/2.0 * (T[i]-T[i+1])/dz
dE2[i]=dE2[i]*dt # Total energy flux into cell "i"
775 Tn[i]=T[i]+dE2[i]/(p_soil*Cp[i]*dz) # conduction calculating the new temperature in the next
cell.
Bnew[i]=B[i] # calculating the new ice/water ratio in the next cell
if dE2[i]<0.0 and Tn[i]<Tfr: #condition that verify the amount of energy and the new temperature.
if the energy gets less than 0 value it means that energy is escaping the cell and it will cool down or
780 freezes.
if B[i]>0.0001: # Freezing
Bnew[i]=B[i]+(dE2[i]-(T[i]-Tfr)*(p[i]*Cp[i]*dz))/(p[i]*L*dz*por[i]) # the Bnew depends on the
amount of energy that has been used to freeze the previous cell - the rest of the energy
if Bnew[i]>0.0: # if the condition is true the new temperature equals freezing temperature.
785 Tn[i]=Tfr
else:
Tn[i]=Tfr+Bnew[i]*(L*por[i])/Cp[i] # if the condition is false (Bnew <0.0) the new temp. equals
the freezing temp.+Bnew.
Bnew[i]=0.
790
if dE2[i]>0.0 and Tn[i]>Tfr:
if B[i]<0.9999: # Thawing
Bnew[i]=B[i]+(dE2[i]-(T[i]-Tfr)*(p[i]*Cp[i]*dz))/(p[i]*L*dz*por[i])
795 if Bnew[i]<1.0:
Tn[i]=Tfr
else:
Tn[i]=Tfr+(Bnew[i]-1.0)*(L*por[i])/Cp[i]
Bnew[i]=1.
800
for i in range(1,n-1):
T[i]=Tn[i]
B[i]=Bnew[i]

```

```

805 plt.plot(T,-x, 'r',label="Temperature",linewidth=0.5)

#exporting data to csv file. Graphs was created with Microsoft Excel.
name_dict =
'    Temperature': T,[:0]
810 '    time':time,[:0]
'    depth': Depth,[:0]
'    B': B,[:0]
'    K': K,[:0]
'    Cp': Cp,[:0]
815 '    p': p,[:0]
'    dE2': dE2[:0]
{
df = pd.DataFrame(name_dict)
df.to_csv(r'C:\Users\ADMIN\Desktop\Python    Dotan\1Dmodel_1.csv',mode='a',    header=True,
820 float_format='%.3f') # defines the location of the data exported
pd.read_csv('trial2.csv').count()

#Commands for graph in python script. Graphs for article was created with Microsoft Excel.
axes1 = plt.gca()
825 plt.ylabel('Depth')
plt.legend(loc ="lower left")
plt.grid()
axes2 = axes1.twin()
axes1.set_xlabel("Temperature")
830 plt.plot(B,-x, 'g',linestyle = '--',linewidth=0.7, label="B")
axes2.set_xticks([0., .2, .4, .6, .8, 1.0])
axes2.set_xlabel("B")
plt.legend(loc ="lower left")
plt.show()

```

835

10. Data availability

All raw data can be provided by the corresponding authors upon request.

11. Executable research compendium (ERC)

12. Sample availability

840 **13. Supplement link: the link to the supplement will be included by Copernicus, if applicable.**

14. Author contribution:

DR, YW, and HHC planned the drilling campaign; DR and YW, ~~p~~Processed the cores and lab work in UNIS Svalbard; DR and YH performed the water chemistry analysis at GSI; VL and DR developed the 1-D model; DR, YW and VL wrote the manuscript. [All authors commented on the manuscript.](#)

845 **15. Competing interests:**

The authors declare that they have no conflict of interest.

16. Disclaimer

17. Acknowledgments

850 We would like to acknowledge Ullrich (Ulli) Neuman for leading the 2017 drilling campaign in Adventdalen. Andreas ~~A~~alexander and Graham L. Gilbert for field assistance. Danni Rohdent for lab assistance. Gerd-Irena and UNIS logistics for their assistance with field and laboratory gear. GSI geochemical lab members Olga Berlin, Galit Sharabi and Dina Siber for their assistance with chemistry analysis. Yosi Yechieli for consulting about various issues of the article. The drilling campaign was [supported by an](#)

855 [Arctic Field Grant from the Norwegian Research Council, granted by AFG](#), Project Number: 269988 RiS
ID: 10664.

References

- [Ahonen, L.: Permafrost: occurrence and physiochemical processes \(POSIVA--01-05\). Finland, ISBN 951-652-106-1, 2001.](#)
- 860 Alsos, I. G., Sjögren, P., Edwards, M. E., Landvik, J. Y., Gielly, L., Forwick, M., Coissac E., Brown A.
G., Jakobsen L. V., Føreid M. K., & Pedersen, M. W.: Sedimentary ancient DNA from Lake
Skartjørna, Svalbard: Assessing the resilience of arctic flora to Holocene climate change, *The
Holocene*, 26(4), 627-642, <https://doi.org/10.1177%2F0959683615612563>, 2016.
- Ames, W. F.: Numerical methods for partial differential equations, Second edition, Academic press
INC, 1977.
- 865 Anderson L, Edwards, M, Shapley, M. D., Finney, B. P. and Langdon, C.: Holocene Thermokarst Lake
Dynamics in Northern Interior Alaska: The Interplay of Climate, Fire, and Subsurface Hydrology, *Front.
Earth Sci.* 7:53, <https://doi.org/10.3389/feart.2019.00053>, 2019.
- [Angelopoulos, M., Westermann, S., Overduin, P., Faguet, A., Olenchenko, V., Grosse, G., & Grigoriev,
M. N.: Heat and salt flow in subsea permafrost modeled with CryoGRID2. *Journal of Geophysical
Research: Earth Surface*, 124\(4\), 920-937, <https://doi.org/10.1029/2018JF004823>, 2019.](#)
- 870 -Arnscheidt, C. W. & Rothman, D. H., Routes to global glaciation. *Proceedings of the Royal Society
A*, 476(2239), <https://doi.org/10.1098/rspa.2020.0303>, 2020.
- Bear, J., Cheng, A. H. D., Sorek, S., Ouazar, D., & Herrera, I. (Eds.): *Seawater intrusion in coastal
aquifers: concepts, methods and practices*. Kluwer Academic Publishers pp 591, 1999.
- 875 Bear, J., & Dagan, G.: Some exact solutions of interface problems by means of the hodograph
method, *JGR*, 69(8), 1563-1572, <https://doi.org/10.1029/JZ069i008p01563>, 1964.
- Benn, D., & Evans, D. J.: *Glaciers and glaciation*, Second edition, pp 707, Routledge, 2014.
- Betlem, P., Midttømme, K., Jochmann, M., Senger, K., & Olaussen, S.: Geothermal Gradients on
Svalbard, Arctic Norway. In *First EAGE/IGA/DGMK Joint Workshop on Deep Geothermal Energy* (pp.
880 cp-577). European Association of Geoscientists & Engineers, [https://doi.org/10.3997/2214-
4609.201802945](https://doi.org/10.3997/2214-4609.201802945), 2018.

- Birks, H. H.: Holocene vegetational history and climatic change in west Spitsbergen-plant macrofossils from Skardtjørna, an Arctic lake, *The Holocene*, 1(3), 209-218, <https://doi.org/10.1177/095968369100100303>, 1991.
- 885 Black, R. F.: Permafrost: a review, *GSA Bulletin*, 65(9), 839-856, [https://doi.org/10.1130/0016-7606\(1954\)65\[839:PR\]2.0.CO;2](https://doi.org/10.1130/0016-7606(1954)65[839:PR]2.0.CO;2), 1954.
- Bodnar, R. J.: Revised equation and table for determining the freezing point depression of H₂O-NaCl solutions. *GCA*, 57(3), 683-684, <http://www.osti.gov/scitech/biblio/6951353>, 1993.
- Bockheim, J. G., & Hall, K. J.: Permafrost, active-layer dynamics and periglacial environments of continental Antarctica: periglacial and permafrost research in the Southern Hemisphere, *S. Afr. J. Sci.*, 98(1), 82-90, <https://hdl.handle.net/10520/EJC97385>, 2002.
- Burn, C. R.: Permafrost distribution and stability, edited by: French, H., & Slaymaker, O., *Changing Cold Environments: A Canadian Perspective*, John Wiley & Sons, Ltd, 126-143, <https://doi.org/10.1002/9781119950172.ch7>, 2011.
- 895 Burt, T. P., & Williams, P. J.: Hydraulic conductivity in frozen soils, *Earth Surface Processes*, 1(4), 349-360, <https://doi.org/10.1002/esp.3290010404>, 1976.
- Cable, S., Elberling, B., & Kroon, A.: Holocene permafrost history and cryostratigraphy in the High-Arctic Adventdalen Valley, central Svalbard. *Boreas*, 47(2), 423-442, <https://doi.org/10.1111/bor.12286>, 2018.
- 900 Cary, J. W., & Mayland, H. F.: Salt and water movement in unsaturated frozen soil. *Soil Science Society of America Journal*, 36(4), 549-555, <https://doi.org/10.2136/sssaj1972.03615995003600040019x>, 1972.
- Cascoyne, M.: A review of published literature on the effects of permafrost on the hydrogeochemistry of bedrock, Technical Report, Posiva Oy, Helsinki Finland, 2000.
- 905 Christiansen, H. H.: Thermal regime of ice-wedge cracking in Adventdalen, Svalbard. *PERMAFROST PERIGLAC*, 16(1), 87-98, <https://doi.org/10.1002/ppp.523>, 2005.
- Christiansen, H. H., Etzelmüller, B., Isaksen, K., Juliussen, H., Farbrot, H., Humlum, O., Johansson, M., Ingeman-Nielsen, T., Kristensen, L., Hjort, J., Holmlund, P. Sannel, A. B. K. Sigsgaard, C. Åkerman, H. J. Foged, N. Blikra, L. H. Pernosky, M. A. & Ødegård, R. S.: The thermal state of permafrost in the Nordic area during the International Polar Year 2007–2009. *PERMAFROST PERIGLAC*, 21(2), 156-181, <https://doi.org/10.1002/ppp.687>, 2010.
- 910

- Christiansen, H. H., French, H. M., & Humlum, O.: Permafrost in the Gruve-7 mine, Adventdalen, Svalbard. *NORSK GEOGR TIDSSKR*, 59(2), 109-115, <https://doi.org/10.1080/00291950510020592>, 2005.
- 915 [Christiansen, H.H., Gilbert, G.L., Demidov, N., Guglielmin, M., Isaksen, K., Osuch, M. & Boike, J.: Permafrost temperatures and active layer thickness in Svalbard 2017-2018. *State of Environmental Science in Svalbard*, Van den Heuvel F, Hübner C, Błaszczuk M, Heimann M, Lihavainen H \(eds\) 2020: SESS report 2019, Longyearbyen, Svalbard Integrated Arctic Earth Observing System, Report card, p. 236-249, 10013/epic.b4472816-40ba-4089-9ce7-d7539e10e0a3, 2020.](#)
- 920 [Christiansen, H. H., Etzelmüller, B., Isaksen, K., Juliussen, H., Farbrøt, H., Humlum, O., Johansson, M., Ingeman-Nielsen, T., Kristensen, L., Hjort, J., Holmlund, P., Sannel, A. B. K., Sigegaard, C., Åkerman, H. J., Foged, N., Blikra, L. H., Pernesky, M. A. & Ødegård, R. S.: The thermal state of permafrost in the Nordic area during the International Polar Year 2007–2009. *PERMAFROST PERIGLAC*, 21\(2\), 156–181, <https://doi.org/10.1002/ppp.687>, 2010.](#)
- 925 Christiansen, H. H., Humlum, O., & Eckerstorfer, M.: Central Svalbard 2000–2011 meteorological dynamics and periglacial landscape response, *ARCT ANTARCT ALP RES*, 45(1), 6-18, <https://doi.org/10.1657/1938-4246-45.16>, 2013.
- Cocks, F. H., & Brower, W. E.: Phase diagram relationships in cryobiology, *CRYOBIOLOGY*, 11(4), 340-358, [https://doi.org/10.1016/0011-2240\(74\)90011-X](https://doi.org/10.1016/0011-2240(74)90011-X), 1974.
- 930 Cochand, M., Molson, J., & Lemieux, J. M.: Groundwater hydrogeochemistry in permafrost regions, *PERMAFROST PERIGLAC*, 30(2), 90-103, <https://doi.org/10.1002/ppp.1998>, 2019.
- Crank, J.: Free and moving boundary problems. Oxford University Press, USA, 1984.
- Dobinski, W.: Permafrost. *EARTH-SCI REV*, 108(3-4), 158-169, <https://doi.org/10.1016/j.earscirev.2011.06.007>, 2011.
- 935 [de Baar, H.J.W., van Heuven, S.M.A.C., Middag, R. : Ocean Salinity, Major Elements, and Thermohaline Circulation. In: White, W. \(eds\) *Encyclopedia of Geochemistry. Encyclopedia of Earth Sciences Series*. Springer, Cham. \[https://doi.org/10.1007/978-3-319-39193-9_120-1\]\(https://doi.org/10.1007/978-3-319-39193-9_120-1\), 2017.](#)
- Edmunds, W. M., Hinsby, K., Marlin, C., de Melo, M. C., Manzano, M., Vaikmae, R., & Travi, Y.: Evolution of groundwater systems at the European coastline. *GEOL SOC SP*, London, 189(1), 289-311, <https://doi.org/10.1144/GSL.SP.2001.189.01.17>, 2001.
- 940 El Kadi, K., & Janajreh, I.: Desalination by freeze crystallization: an overview, *Int. J. Therm. Environ. Eng*, 15(2), 103-110, Doi: 10.5383/ijtee.15.02.004, 2017.

- Elverhøi, A., Svendsen, J. I., Solheim, A., Andersen, E. S., Milliman, J., Mangerud, J., & Hooke, R. L.: Late Quaternary sediment yield from the high Arctic Svalbard area. *The Journal of Geology*, 103(1), 1-17, <https://www.jstor.org/stable/30071132>, 1995.
- 945 Etzelmüller, B., Schuler, T. V., Isaksen, K., Christiansen, H. H., Farbrot, H., and Benestad, R.: Modeling the temperature evolution of Svalbard permafrost during the 20th and 21st century, *The Cryosphere*, 5, 67–79, <https://doi.org/10.5194/tc-5-67-2011>, 2011.
- Farbrot, H., Etzelmüller, B., Schuler, T. V., Guðmundsson, Á., Eiken, T., Humlum, O., & Björnsson, H.: Thermal characteristics and impact of climate change on mountain permafrost in Iceland. *J GEOPHYS RES-EARTH*, 112(F3), <https://doi.org/10.1029/2006JF000541>, 2007.
- 950 Farnsworth, W. R. The Topographical and Meteorological Influence on Snow Distribution in Central Spitsbergen: How the spatial variability of snow influences slope-scale stability, permafrost landform dynamics and regional distribution trends *The Topographical and Meteorological Influence on Snow Distribution in Central Svalbard*. Master Thesis, department of geosciences faculty of mathematics and natural sciences university of Oslo, 2013.
- 955 Farnsworth, W. R., Ingólfsson, Ó., Alexanderson, H., Allaart, L., Forwick, M., Noormets, R., Retelle, M. & Schomacker, A.: Holocene glacial history of Svalbard: Status, perspectives and challenges, *EARTH-SCI REV*, 103249, <https://doi.org/10.1016/j.earscirev.2020.103249>, 2020.
- 960 Farouki, O. T.: Thermal properties of soils. Cold Regions Research and Engineering Lab Hanover NH., 1981.
- Forman, S. L., Lubinski, D. J., Ingólfsson, Ó., Zeeberg, J. J., Snyder, J. A., Siegert, M. J., & Matishov, G. G. (2004). A review of postglacial emergence on Svalbard, Franz Josef Land and Novaya Zemlya, northern Eurasia. *QUATERNARY SCI REV*, 23(11-13), 1391-1434, <https://doi.org/10.1016/j.quascirev.2003.12.007>, 2004.
- 965 French, H. M.: The periglacial environment, fourth edition, John Wiley & Sons LTD, 2017.
- Gilbert, G. L., Christiansen, H. H., & Neumann, U.: Coring of unconsolidated permafrost deposits: methodological successes and challenges, In *Proceedings GeoQuébec 2015 – 68th Canadian Geotechnical Conference and 7th Canadian Permafrost Conference*, 20–23, Québec, Canada. Paper 6
- 970 pp. <https://hdl.handle.net/1956/17626>, 2015.
- Gilbert, G. L., O'Neill, H. B., Nemeč, W., Thiel, C., Christiansen, H. H., & Buylaert, J. P.: Late Quaternary sedimentation and permafrost development in a Svalbard fjord-valley, Norwegian high Arctic. *Sedimentology*, 65(7), 2531-2558, <https://doi.org/10.1111/sed.12476>, 2018.

- 975 Gilbert, G., Instanes, A., Sinitsyn, A., & Aalberg, A.: Characterization of two sites for geotechnical testing in permafrost: Longyearbyen, Svalbard. <http://hdl.handle.net/11250/2632119>, 2019.
- Gitterman, K. E.: Thermal analysis of seawater. CRREL TL, 287, 1937.
- Grinter, M., Lacelle, D., Baranova, N., Murseli, S., & Clark, I. D.: Late Pleistocene and Holocene ice-wedge activity on the Blackstone Plateau, central Yukon, Canada. QUATERNARY RES, 1–15. <https://doi.org/10.1017/qua.2018.65>, 2018.
- 980 rünberg, I., Wilcox, E. J., Zwieback, S., Marsh, P., and Boike, J.: Linking tundra vegetation, snow, soil temperature, and permafrost, Biogeosciences, 17, 4261–4279, <https://doi.org/10.5194/bg-17-4261-2020>, 2020.
- Grundvåg, S. A., Jelby, M. E., Śliwińska, K. K., Nøhr-Hansen, H., Aadland, T., Sandvik, S. E., Tennvassås, I., Engen, T., & Olaussen, S.: Sedimentology and palynology of the Lower Cretaceous
- 985 succession of central Spitsbergen: integration of subsurface and outcrop data. NORW J GEOL, 99(2):253-284, <https://dx.doi.org/10.17850/njg99-2-02>, 2019.
- Harada, K., & Yoshikawa, K.: Permafrost age and thickness near Adventfjorden, Spitsbergen. Polar Geography, 20(4), 267-281, <https://doi.org/10.1080/10889379609377607>, 1996.
- Herut, B., Starinsky, A., Katz, A., & Bein, A.: The role of seawater freezing in the formation of
- 990 subsurface brines. GEOCHIM COSMOCHIM AC, 54(1), 13-21, [https://doi.org/10.1016/0016-7037\(90\)90190-V](https://doi.org/10.1016/0016-7037(90)90190-V), 1990.
- Homshaw, L. G.: Freezing and melting temperature hysteresis of water in porous materials: Application to the study of pore form, J SOIL SCI, 31(3), 399-414, <https://doi.org/10.1111/j.1365-2389.1980.tb02090.x>, 1980.
- 995 Hornum, M. T., Hodson, A. J., Jessen, S., Bense, V., and Senger, K.: Numerical modelling of permafrost spring discharge and open-system pingo formation induced by basal permafrost aggradation, The Cryosphere, 14, 4627–4651, <https://doi.org/10.5194/tc-14-4627-2020>, 2020.
- [Hornum, M. T., Betlem, P., & Hodson, A.: Groundwater flow through continuous permafrost along geological boundary revealed by electrical resistivity tomography. Geophysical Research Letters, 48\(14\), https://doi.org/10.1029/2021GL092757, 2021.](https://doi.org/10.1029/2021GL092757)
- 1000 Humlum, O., Instanes, A., & Sollid, J. L.: Permafrost in Svalbard: a review of research history, climatic background and engineering challenges. POLAR RES, 22(2), 191-215, <https://doi.org/10.1111/j.1751-8369.2003.tb00107.x>, 2003.

- 1005 Humlum, O.: Holocene permafrost aggradation in Svalbard. *GEOL SOC SPEC PUBL*, London, 242(1), 119-129, <https://doi.org/10.1144/GSL.SP.2005.242.01.11>, 2005.
- Imbrie, J., Berger, A., Boyle, E., Clemens, S. C., Duffy, A., Howard, W. R., Kukla, G., Kutzbach, J., Martinson, D. G., McIntyre, A., Mix, A. C., Molfino, B., Morley, J. J., Peterson, L. C., Pisias, N. G., Prell, M. E., Raymo, W. L., Shackleton, N. J. & Toggweiler, J. R.: On the structure and origin of major glaciation cycles 2. The 100,000-year cycle. *Paleoceanography*, 8(6), 699-735, <https://doi.org/10.1029/93PA02751>, 1993.
- 1010 Isaksen, K., Benestad, R. E., Harris, C., & Sollid, J. L.: Recent extreme near-surface permafrost temperatures on Svalbard in relation to future climate scenarios. *Geophys Res Lett*, 34(17), <https://doi.org/10.1029/2007GL031002>, 2007.
- Iwahana, G., Cooper, Z. S., Carpenter, S. D., Deming, J. W., & Eicken, H. (2021). Intra-ice and intra-sediment cryopeg brine occurrence in permafrost near Utqiaġvik (Barrow). *Permafrost and Periglacial Processes*, 32(3), 427-446. <https://doi.org/10.1002/ppp.2101>, 2021.
- 1015 Kasprzak, M., Łopuch, M., Glowacki, T., & Milczarek, W.: Evolution of near-shore outwash fans and permafrost spreading under their surface: A case study from Svalbard, *Remote Sens-Basel*, 12(3), 482, <https://doi.org/10.3390/rs12030482>, 2020.
- 1020 Kaufman, D. S., Axford, Y. L., Henderson, A. C., McKay, N. P., Oswald, W. W., Saenger, C., Anderson, R. S., Bailey, H. L., Clegg, B., Gajewski, K., Hu, F. S., Jones, M. C., Massa, C., Routson, C. C., Werner, A., Wooller, M. J., & Yu, Z.: Holocene climate changes in eastern Beringia (NW North America)—A systematic review of multi-proxy evidence, *Quaternary Sci Rev*, 147, 312-339, <https://doi.org/10.1016/j.quascirev.2015.10.021>, 2016.
- 1025 Keating, K., Binley, A., Bense, V., Van Dam, R. L., & Christiansen, H. H.: Combined geophysical measurements provide evidence for unfrozen water in permafrost in the Adventdalen valley in Svalbard. *Geophys Res Lett*, 45(15), 7606-7614, <https://doi.org/10.1029/2017GL076508>, 2018.
- Kjellman, S. E., Schomacker, A., Thomas, E. K., Håkansson, L., Duboscq, S., Cluett, A. A., Farnsworth, W. R., Allaart L., Cowling, O. C., McKay, N. P., Brynjólfsson, S., & Ingólfsson, Ó.: Holocene precipitation seasonality in northern Svalbard: influence of sea ice and regional ocean surface conditions. *Quaternary Sci Rev*, 240, 106388, <https://doi.org/10.1016/j.quascirev.2020.106388>, 2020.

- 1035 [Kokelj, S. V., Smith, C. A. S., & Burn, C. R.: Physical and chemical characteristics of the active layer and permafrost, Herschel Island, western Arctic Coast, Canada. *Permafrost and Periglacial Processes*, 13\(2\), 171-185, <https://doi.org/10.1002/ppp.417>, 2002.](#)
- Kukkonen, I. T., & Šafanda, J.: Numerical modelling of permafrost in bedrock in northern Fennoscandia during the Holocene. *Global and Planet Change*, 29(3-4), 259-273, [https://doi.org/10.1016/S0921-8181\(01\)00094-7](https://doi.org/10.1016/S0921-8181(01)00094-7), 2001.
- 1040 Kutzbach, J. E., & Guetter, P. J.: The influence of changing orbital parameters and surface boundary conditions on climate simulations for the past 18 000 years. *Journal of atmospheric sciences*, 43(16), 1726-1759, [https://doi.org/10.1175/1520-0469\(1986\)043<1726:TIOCOP>2.0.CO;2](https://doi.org/10.1175/1520-0469(1986)043<1726:TIOCOP>2.0.CO;2), 1986.
- Landvik, J. Y., Landvik, J. Y., & Salvigsen, O.: The Late Weichselian and Holocene shoreline displacement on the west-central coast of Svalbard. *Polar Res*, 5(1), 29-44, <https://doi.org/10.1111/j.1751-8369.1987.tb00353.x>, 1987.
- 1045 Landvik, J. Y., Mangerud, J., & Salvigsen, O.: Glacial history and permafrost in the Svalbard area. In *Proceedings of the 5th International Conference on Permafrost* (Vol. 1, pp. 194-198), Trondheim, Tapir Publishers., 1988.
- Lemieux, J. M., Sudicky, E. A., Peltier, W. R., & Tarasov, L.: Simulating the impact of glaciations on continental groundwater flow systems: 1. Relevant processes and model formulation. *J Geophys Res-*
- 1050 *Earth*, 113(F3), <https://doi.org/10.1029/2007JF000928>, 2008.
- Lenz, J., Grosse, G., Jones, B. M., Walter Anthony, K. M., Bobrov, A., Wulf, S., & Wetterich, S.: Mid-Wisconsin to Holocene Permafrost and Landscape Dynamics based on a Drained Lake Basin Core from the Northern Seward Peninsula, Northwest Alaska. *Permafrost Periglac*, 27(1), 56–75. <https://doi.org/10.1002/ppp.1848>, 2015.
- 1055 Lønne, I., & Lyså, A.: Deglaciation dynamics following the Little Ice Age on Svalbard: implications for shaping of landscapes at high latitudes. *Geomorphology*, 72(1-4), 300-319, <https://doi.org/10.1016/j.geomorph.2005.06.003>, 2005.
- Lønne, I., & Nemeč, W.: High-arctic fan delta recording deglaciation and environment disequilibrium. *Sedimentology*, 51(3), 553-589, <https://doi.org/10.1111/j.1365-3091.2004.00636.x>, 2004.
- 1060 Lunardini, V. J.: Freezing of soil with an unfrozen water content and variable thermal properties (Vol. 88, No. 2). US Army Corps of Engineers, Cold Regions Research & Engineering Laboratory, 1988.

- 1065 Luo, D., Jin, H., Marchenko, S. S., & Romanovsky, V. E.: Difference between near-surface air, land surface and ground surface temperatures and their influences on the frozen ground on the Qinghai-Tibet Plateau. *Geoderma*, 312, 74-85., <https://doi.org/10.1016/j.geoderma.2017.09.037>, 2018.
- Lüthi, Z. L.: Thermal State of Permafrost in Central and Western Spitsbergen 2008-2009, Master's Thesis Faculty of Science University of Bern, 2010.
- 1070 Nordli, Ø., Przybylak, R., Ogilvie, A. E., & Isaksen, K.: Long-term temperature trends and variability on Spitsbergen: the extended Svalbard Airport temperature series, 1898–2012. *Polar res*, 33(1), 21349, <https://doi.org/10.3402/polar.v33.21349>, 2014.
- <http://repozytorium.umk.pl/handle/item/6323>, 2020.
- [Nordli, Ø., Wyszynski, P., Gjelten, H., Isaksen, K., Łupikasza, E., Niedźwiedz, T., & Przybylak, R.: Revisiting the extended Svalbard Airport monthly temperature series, and the compiled corresponding daily series 1898–2018, http://repozytorium.umk.pl/handle/item/6323, 2020.](http://repozytorium.umk.pl/handle/item/6323)
- 1075 Major, H., & Nagy, J.: Geology of the Adventdalen map area: with a geological map, Svalbard C9G 1: 100 000, Norsk Polarinsittutt, Oslo, 1972.
- McKenzie, J. M., Voss, C. I., & Siegel, D. I.: Groundwater flow with energy transport and water–ice phase change: numerical simulations, benchmarks, and application to freezing in peat bogs. *Adv water resour*, 30(4), 966-983, <https://doi.org/10.1016/j.advwatres.2006.08.008>, 2007.
- 1080 Mangerud, J., Bolstad, M., Elgersma, A., Helliksen, D., Landvik, J. Y., Lønne, I., Lycke, A. K., Salvigsen, O., Sandahl, T., & Svendsen, J. I.: The last glacial maximum on Spitsbergen, Svalbard. *Quaternary Res*, 38(1), 1-31, [https://doi.org/10.1016/0033-5894\(92\)90027-G](https://doi.org/10.1016/0033-5894(92)90027-G), 1992.
- Mangerud, J., Astakhov, V., & Svendsen, J. I.: The extent of the Barents–Kara ice sheet during the Last Glacial Maximum, *Quaternary Sci Rev*, 21(1-3), 111-119, [https://doi.org/10.1016/S0277-3791\(01\)00088-9](https://doi.org/10.1016/S0277-3791(01)00088-9), 2002.
- 1085 Mangerud, J., & Svendsen, J. I.: The Holocene thermal maximum around Svalbard, Arctic North Atlantic; molluscs show early and exceptional warmth, *The Holocene*, 28(1), 65-83, <https://doi.org/10.1177/0959683617715701>, 2018.
- Marion, G. M., Farren, R. E., & Komrowski, A. J.: Alternative pathways for seawater freezing. *Cold Reg Sci Technol*, 29(3), 259-266, [https://doi.org/10.1016/S0165-232X\(99\)00033-6](https://doi.org/10.1016/S0165-232X(99)00033-6), 1999.
- 1090 McEwen, T., & Marsily, G.de.: The potential significance of permafrost to the behaviour of a deep radioactive waste repository, (SKI-TR--91-8). Sweden, 1991.

- McFarlin, J. M., Axford, Y., Osburn, M. R., Kelly, M. A., Osterberg, E. C., & Farnsworth, L. B.: Pronounced summer warming in northwest Greenland during the Holocene and Last Interglacial. *PNAS*, 115(25), 6357-6362, <https://doi.org/10.1073/pnas.1720420115>, 2018.
- 1095 Morgenstern, N. R., & Anderson, D. M.: Physics, chemistry, and mechanics of frozen ground: a review. In *Permafrost: North American Contribution [to The] Second International Conference (Vol. 2, p. 257)*. National Academies, 1973.
- Murton, J. B.: What and where are periglacial landscapes?. *Permafrost Periglac*, 32(2), 186-212, <https://doi.org/10.1002/ppp.2102>, 2021.
- 1100 Nelson, K. H., & Thompson, T. G. (1954). Deposition of salts from sea water by frigid concentration. Obu, J., Westermann, S., Bartsch, A., Berdnikov, N., Christiansen, H. H., Dashtseren, A., Delaloye, R., Elberling, B., Etzelmüller, B., Kholodov, A., Khomutov, A., Kääb, A., Leibman, M. O., Lewkowicz, A. G., Panda, S. K., Romanovsky, V., Way, R. G. Westergaard-Nielsen, A., Wu, T., Yamkhin, J. & Zou, D.: Northern Hemisphere permafrost map based on TTOP modelling for 2000–
- 1105 2016 at 1 km² scale. *Earth-Sci Rev*, 193, 299-316, <https://doi.org/10.1016/j.earscirev.2019.04.023>, 2019.
- Olaussen, S., Senger, K., Braathen, A., Grundvåg, S. A., & Mørk, A.: You learn as long as you drill; research synthesis from the Longyearbyen CO₂ Laboratory, Svalbard, Norway. *Norw J Geol*, 99(2), 157-187, <https://doi.org/10.17850/njg008>, 2019.
- 1110 Oldenborger, G. A., & LeBlanc, A. M.: Monitoring changes in unfrozen water content with electrical resistivity surveys in cold continuous permafrost. *Geophys J Int*, 215(2), 965-977, <https://doi.org/10.1093/gji/ggy321>, 2018.
- Osuch, M., & Wawrzyniak, T.: Inter-and intra-annual changes in air temperature and precipitation in western Spitsbergen. *Int J Climatol*, 37(7), 3082-3097, <https://doi.org/10.1002/joc.4901>, 2017.
- 1115 [Overduin, P. P., Schneider von Deimling, T., Miesner, F., Grigoriev, M. N., Ruppel, C. D., Vasiliev, A., et al.: Submarine permafrost map in the Arctic modeled using 1-D transient heat flux \(SuPerMAP\) *Journal of Geophysical Research: Oceans*, 124, 3490– 3507, <https://doi.org/10.1029/2018JC014675>, 2019.](#)
- 1120 Park, H. S., Kim, S. J., Stewart, A. L., Son, S. W., & Seo, K. H.: Mid-Holocene Northern Hemisphere warming driven by Arctic amplification. *Science advances*, 5(12), eaax8203, <https://www.science.org/doi/abs/10.1126/sciadv.aax8203>, 2019.

- Patton, H., Hubbard, A., Andreassen, K., Auriac, A., Whitehouse, P. L., Stroeven, A. P., Shackleton, C., Winsborrow, M., Heyman, J., & Hall, A. M.: Deglaciation of the Eurasian ice sheet complex. *Quaternary Sci Rev*, 169, 148-172, <https://doi.org/10.1016/j.quascirev.2017.05.019>, 2017.
- 1125 Rasmussen, T. L., Forwick, M., & Mackensen, A.: Reconstruction of inflow of Atlantic Water to Isfjorden, Svalbard during the Holocene: Correlation to climate and seasonality, *Mar Micropaleontol*, 94, 80-90, <https://doi.org/10.1016/j.marmicro.2012.06.008>, 2012.
- Ringer, W. E. *Über die Veränderungen in der Zusammensetzung des Meerwassersalzes beim Ausfrieren*. O. Verlag, 1905.
- 1130 Rubinstein, L., Geiman, H., & Shachaf, M.: Heat transfer with a free boundary moving within a concentrated thermal capacity. *IMA J Appl Math*, 28(2), 131-147, <https://doi.org/10.1093/imamat/28.2.131>, 1982.
- Rühaak, W., Anbergen, H., Grenier, C., McKenzie, J., Kurylyk, B. L., Molson, J., Roux, N., & Sass, I. Benchmarking numerical freeze thaw models. *Energy Procedia*, <https://doi.org/10.1016/j.egypro.2015.07.866>, 2015.
- 1135 Salvigsen, O.: Occurrence of pumice on raised beaches and Holocene shoreline displacement in the inner Isfjorden area, Svalbard, *Polar Res*, 2(1), 107-113, <https://doi.org/10.1111/j.1751-8369.1984.tb00488.x>, 1984.
- Šarler, B.: Stefan's work on solid-liquid phase changes. *Eng Anal Bound Elem*, 16(2), 83-92, [https://doi.org/10.1016/0955-7997\(95\)00047-X](https://doi.org/10.1016/0955-7997(95)00047-X), 1995.
- 1140 Sessford, E. G., Strzelecki, M. C., & Hormes, A.: Reconstruction of Holocene patterns of change in a High Arctic coastal landscape, Southern Sassenfjorden, Svalbard. *Geomorphology*, 234, 98-107, <https://doi.org/10.1016/j.geomorph.2014.12.046>, 2015.
- 1145 Solomon, S. M., Taylor, A. E., & Stevens, C. W.: Nearshore ground temperatures, seasonal ice bonding, and permafrost formation within the bottom-fast ice zone, Mackenzie Delta, NWT. In *Proceedings of the Ninth International Conference on Permafrost, Fairbanks, Alaska (Vol. 29, pp. 1675-1680). Fairbanks: Institute of Northern Engineering, University of Alaska Fairbanks. 2018*
- 1150 Strand, S. M., Christiansen, H. H., Johansson, M., Åkerman, J., & Humlum, O.: Active layer thickening and controls on interannual variability in the Nordic Arctic compared to the circum-Arctic. *Permafrost and Periglacial Processes*, 32(1), 47-58. <https://doi.org/10.1002/ppp.2088>, 2021.

- Szafranec, J. E., & Dobiński, W.: Deglaciation rate of selected Nunataks in Spitsbergen, Svalbard—Potential for permafrost expansion above the glacial environment, *Geosciences*, 10(5), 202. <https://doi.org/10.3390/geosciences10050202>, 2020.
- 1155 Tavakoli, S., Gilbert, G., Lysdahl, A. O. K., Frauenfelder, R., & Forsberg, C. S.: Geoelectrical properties of saline permafrost soil in the Adventdalen valley of Svalbard (Norway), constrained with in-situ well data. *Journal of Applied Geophysics*, 195, 104497, <https://doi.org/10.1016/j.jappgeo.2021.104497>, 2021.
- Treat, C. C., & Jones, M. C.: Near-surface permafrost aggradation in Northern Hemisphere peatlands shows regional and global trends during the past 6000 years. *The Holocene*, 28(6), 998-1010, <https://doi.org/10.1177/0959683617752858>, 2018.
- 1160 Ulrich, M., Wetterich, S., Rudaya, N., Frolova, L., Schmidt, J., Siegert, C., Fedorov A. N., & Zielhofer, C.: Rapid thermokarst evolution during the mid-Holocene in Central Yakutia, Russia, *The Holocene*, 27(12), 1899–1913, <https://doi.org/10.1177/0959683617708454>, 2017.
- van der Bilt, W. G., D'Andrea, W. J., Werner, J. P., & Bakke, J.: Early Holocene temperature oscillations exceed amplitude of observed and projected warming in Svalbard lakes, *Geophys Res Lett*, 46(24), 14732-14741, <https://doi.org/10.1029/2019GL084384>, 2019.
- 1165 van der Bilt, W. G., D'Andrea, W. J., Bakke, J., Balascio, N. L., Werner, J. P., Gjerde, M., & Bradley, R. S.: Alkenone-based reconstructions reveal four-phase Holocene temperature evolution for High Arctic Svalbard, *Quaternary Sci Rev*, 183, 204-213, <https://doi.org/10.1016/j.quascirev.2016.10.006>, 2018.
- 1170 Van Everdingen R. V.,: Multi-language glossary of permafrost and related ground-ice terms, Boulder, CO: National Snow and Ice DataCenter/World Data Center for Glaciology; Revised January 2005:98, 1998.
- Verruijt, A.: A note on the Ghyben-Herzberg formula, *Hydrolog Sci J*, 13(4), 43-46, <https://doi.org/10.1080/02626666809493624>, 1968.
- 1175 Waller, R. I., Murton, J. B., & Kristensen, L.: Glacier–permafrost interactions: Processes, products and glaciological implications. *Sediment Geol*, 255, 1-28, <https://doi.org/10.1016/j.sedgeo.2012.02.005>, 2012.
- Walvoord, M. A., & Kurylyk, B. L.: Hydrologic impacts of thawing permafrost—A review. *Vadose Zone J*, 15(6), <https://doi.org/10.2136/vzj2016.01.0010>, 2016.

- 1180 Wohlfarth, B., Lemdahl, G., Olsson, S., Persson, T., Snowball, I., Ising, J., & Jones, V.: Early Holocene environment on Bjørnøya (Svalbard) inferred from multidisciplinary lake sediment studies, *Polar Res*, 14(2), 253-275, <https://doi.org/10.1111/j.1751-8369.1995.tb00693.x>, 1995.
- Weinstein, Y., Rotem, D., Kooi, H., Yechieli, Y., Sültenfuß, J., Kiro, Y., Harlavan, Y., Feldman, M., & Christiansen, H. H.: Radium isotope fingerprinting of permafrost-applications to thawing and intra-
1185 permafrost processes. *Permafrost Periglac*, 30(2), 104-112, <https://doi.org/10.1002/ppp.1999>, 2019.
- [Williams, P. J., & Smith, M. W. \(1989\). *The frozen earth: fundamentals of geocryology* \(Vol. 306\). Cambridge: Cambridge University Press.](#)
- Yang, B., Bai, F., Wang, Y., & Wang, Z.: How mushy zone evolves and affects the thermal behaviours in latent heat storage and recovery: A numerical study, *Int J Energ Res*, 44(6), 4279-4297,
1190 <https://doi.org/10.1002/er.5191>, 2020.
- Zhang, T. Influence of the seasonal snow cover on the ground thermal regime: An overview. *Reviews of Geophysics*, 43(4), <https://doi.org/10.1029/2004RG000157>, 2005